

We are IntechOpen, the world's leading publisher of Open Access books Built by scientists, for scientists

6,900

Open access books available

185,000

International authors and editors

200M

Downloads

Our authors are among the

154

Countries delivered to

TOP 1%

most cited scientists

12.2%

Contributors from top 500 universities



WEB OF SCIENCE™

Selection of our books indexed in the Book Citation Index
in Web of Science™ Core Collection (BKCI)

Interested in publishing with us?
Contact book.department@intechopen.com

Numbers displayed above are based on latest data collected.
For more information visit www.intechopen.com



Tailoring the Kinetic Behavior of Hydride Forming Materials for Hydrogen Storage

Julián Atilio Puszkiel

Abstract

Hydride forming materials, i.e., binary, complex hydrides, and their mixtures, have been extensively investigated owing to their potential hydrogen storage properties. They possess high volumetric hydrogen capacity and relative high gravimetric hydrogen capacity. However, one of the main constraints for their practical application is their slow kinetic behavior. For this reason, enormous effort has been devoted to improve the hydrogenation and dehydrogenation rates. Several strategies have been developed for the enhancement of the kinetic behavior of the most relevant hydride forming materials such as MgH_2 , MBH_4 ($\text{M} = \text{Li, Ca, Mg, Na, K}$), MNH_2 ($\text{M} = \text{Li and Mg}$), $\text{MBH}_4 + \text{'MH}_2$ ($\text{M} = \text{Li, Ca, Mg}$; $\text{'M} = \text{Li, Mg, Ca}$), and $\text{MNH}_2 + \text{'MH}_2$ ($\text{M} = \text{Li, Mg}$; $\text{'M} = \text{Li}$). Tuning the kinetic behavior of these hydride forming materials involves different approaches and their combinations. The most relevant approaches are: (1) improving the microstructural refinement *via* mechanical milling, (2) doping with transition metal and transition metal compounds, (3) forming *in situ* catalyst, and (4) nanoconfining doped hydride forming materials. Herein, basic concepts about the chemical reaction for the hydride compound formation/decomposition, thermodynamics, kinetics, and applied strategies to enhance the kinetic behavior of hydride compounds and systems are comprehensively described and discussed.

Keywords: kinetic behavior, hydrogen storage, hydrides, catalyst, modeling

1. Introduction

1.1 Hydrogen as the future renewable energy vector

In the last two centuries, the energy supply has been based on fossil fuels (natural gas, liquid fuels, and coal). This strong dependence of our modern society on fossil fuels has economic- and geo-political consequences and causes detrimental environmental footprints. **Figure 1A** shows the world fossil fuel demand-supply trend from the 1990s until 2017. In 2017, the world fossil fuel demand (97.8 barrel per day) is over the supply (97.4 barrel per day) [1]. For these reasons, in the last decades, many efforts have been put for the development and research of energy renewable sources. The market of the renewable energies achieved a new global record in 2015 with \$285 billion investment on this technology, exceeding the previous record of \$278 billion on 2011 [2]. The use of renewable energy has many

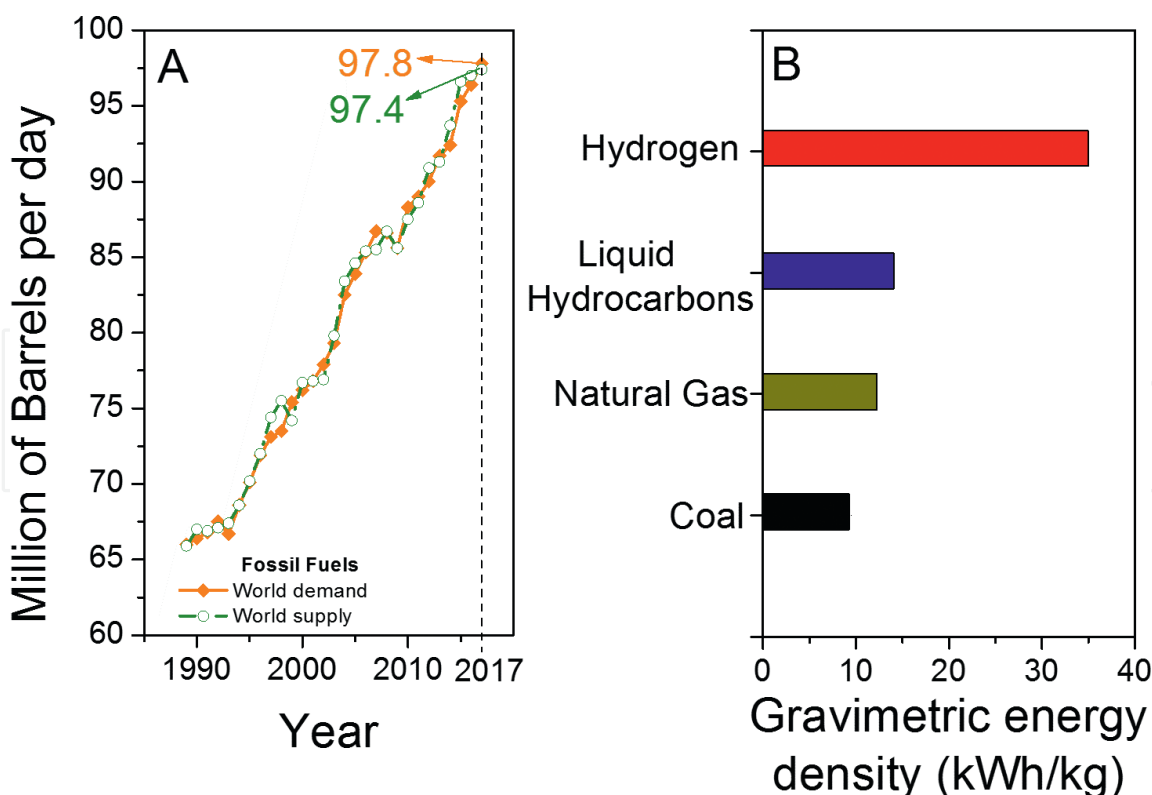


Figure 1.

(A) Evolution of the world demand and supply of fossil fuels in millions of barrels per day (includes all kinds of fossil fuels) [1] and (B) Gravimetric energy density for pure: hydrogen, liquid hydrocarbons, natural gas and coal [3].

potential benefits, including a reduction in CO₂ emissions, the diversification of energy vectors, and a reduced dependency on fossil fuel markets. In this regard, hydrogen (H₂) is considered as a potential energy vector because it is abundant and its combustion generates a large amount of energy and water: $\text{H}_2 + \frac{1}{2} \text{O}_2 \rightarrow \text{H}_2\text{O} + \text{Energy}$. **Figure 1B** shows that H₂ exhibits far higher gravimetric energy density than other traditional fossil fuels: 33.3 kWh/kg for H₂, 13.9 kWh/kg for natural gas, and 12.4 kWh/kg for liquid hydrocarbons [3–6]. Furthermore, H₂ can be directly produced from clean sources such as, for instance, from electrolysis of water or from biomass with light from the sun and biological micro-organism. These renewable methods for hydrogen production can avoid the coal reforming, though this technology is under development and it is not available on industrial scale yet [7].

Nowadays, H₂ is used as feedstock in the petrochemical and fertilizers industries. There are restricted technological applications of H₂ as for example in portable devices like mobile phones, computers, and even some hydrogen driven cars. In spite of all the advantages of H₂ to be considered as the new energy carrier and the evolution of the hydrogen technology showing some technological applications, there are some major issues to be solved before introducing the “hydrogen technology” into the massive market [8]. The hydrogen technology is still under early research and development phase, the current costs of this new technology and the lack of established infrastructure are the main constraints [9–11]. Among the technological problems for the implementation of the “hydrogen economy,” one of the main bottleneck is the lack of safe, compact, energetic-, and cost-efficient hydrogen storage system, especially for mobile applications such as means of transports [12, 13].

On one hand, H₂ has the highest gravimetric energy density in comparison with the traditional fossil fuels, **Figure 1B**. On the other hand, H₂ has extremely low density at room temperature (0.089 g/dm³ under 1 bar), hence its volumetric

energy density is extremely low (0.003 kWh/dm^3). **Figure 2A** shows that the volumetric energy density of H_2 is notably lower than the traditional fossil fuels (0.008 kWh/dm^3 for natural gas, 10.5 kWh/dm^3 for liquid hydrocarbons, and 35 kWh/dm^3 for processed coal). **Figure 2B** shows the volumetric storage density for different traditional and hydrogen storage systems. As seen, there is a huge gap between the volumetric energy density of the light and cheap tank system for liquid hydrocarbons such as gasoline and the volumetric energy density of hydrogen storage systems.

Liquefaction and compression are the traditional physical methods to store hydrogen. Nowadays, available liquid hydrogen storage systems can achieve energy densities of 1.2 kWh/dm^3 . However, cryogenic hydrogen storage systems work at -253°C (liquefied hydrogen temperature) and this requires 20–30% of its energy content. Moreover, hydrogen losses because of evaporation are between 0.3 and 3% per day. On the contrary, gas storage systems can confine hydrogen for long periods without losses. The gas hydrogen vessels need similar technology and infrastructure to that of the established compressed natural gas tanks. Reinforced gas hydrogen containers for 350 and 700 bar of pressure are commercially available. These gas storage systems can achieve volumetric energy densities up to 0.9 kWh/dm^3 , but about 15% of the fuel energy content is required for compression. Solid storage systems in hydride compounds are so far tested on small and middle scale in laboratories. As an example, a tested solid storage system has lower volumetric energy density (0.8 kWh/dm^3) than the traditional physical storage systems [14]. However, solid storage systems work at milder temperature and pressure conditions than the physical storage systems, i.e., in the range of temperatures between 25 and 400°C and under pressure in the range of 10 – 100 bar of H_2 , depending on the hydride material. This means that extreme cryogenic temperature of -253°C or extreme high pressure of 700 bar is not necessary. It brings two main advantages from the safety and energy point of view: (1) mechanical properties of the vessel's material are not demanding as for gas storage containers, (2) energy losses because of hydrogen liquefaction, compression, or boil-off are avoided. Nonetheless, the volumetric energy density of the solid storage hydrogen system is still low, particularly comparing with the gasoline storage system. Moreover, there are critical topics like materials' properties (hydride material), charging and discharging conditions of the systems (pressure, time, and heat transfer), charging

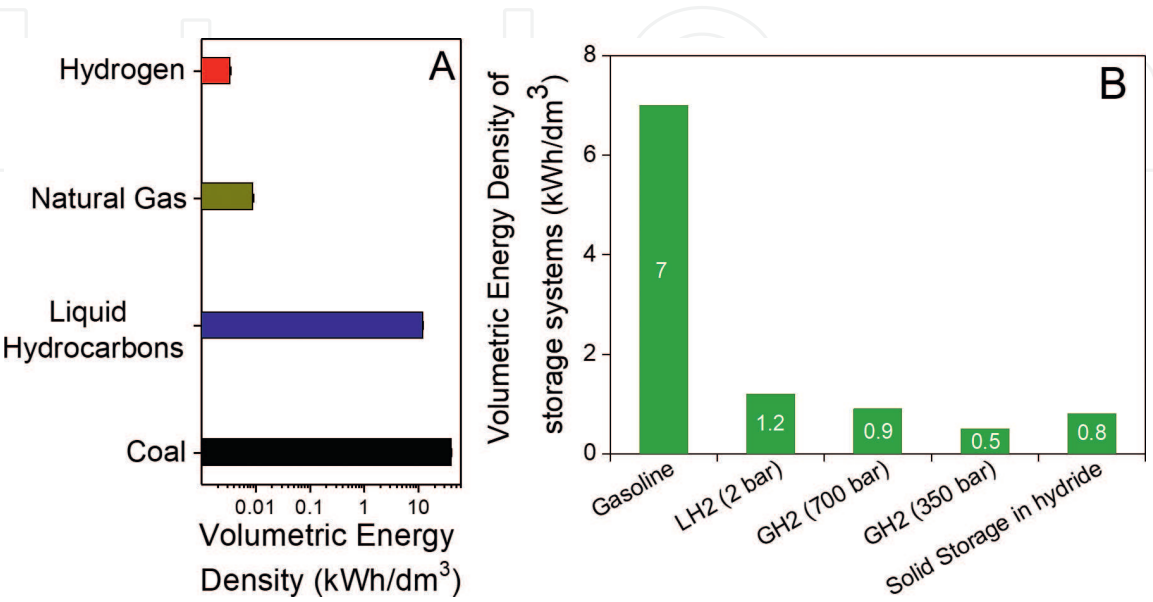


Figure 2.
(A) Volumetric energy density for pure: hydrogen, liquid hydrocarbons, natural gas, and coal [3].
(B) Volumetric energy density for storage systems [14].

cycles, and cost that are still matter of intensive research. Improving mainly the properties of the hydride forming material and optimizing the weight and operative conditions of the solid hydrogen storage system is challenging. However, there are several promising materials under research and development, and besides unexplored system configurations, which can lead to an efficient and safe hydrogen storage system for the future hydrogen economy.

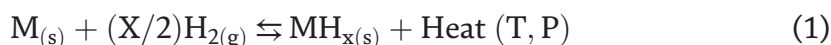
2. Hydride compounds: basics on the chemical reaction and thermodynamics

The solid storage system is based on hydride forming materials, i.e., the system consists basically in a vessel filled with the hydride forming material. Of course, the complexity of the storage system including pipes, heat transfer system, and control instrumentations is in this simplified description neglected. In this section, it is presented basic concepts regarding the chemical reaction for the hydride formation and its thermodynamics.

2.1 Reversible gas: solid chemical reaction

Hydrogen interacts with a large number of elements and materials for the formation of hydride compounds. Hydride forming materials can be classified as: metals (alkaline, alkaline earth, transition, and rare earth), intermetallic (Mg_2Ni , LaNi_5 , etc.), non-intermetallic (Mg-Fe , Mg-Co , etc.), and the combination of boron (B), aluminum (Al), or nitrogen (N) with alkaline or alkaline earth metals. Furthermore, a general classification considering the main feature of different hydride compounds is shown in **Table 1**. There are two main groups of hydride: the room temperature hydrides where hydrogen is located in the interstices of the metal's lattice, without forming a strong metal-hydrogen bond. This kind of hydride works at low temperatures, i.e., 20–50°C, and under low and high pressures, depending on the type of alloy. For instance, LaNi_5 alloy works at low pressure, between 10 and 50 bar, while TiCrMo alloy uptake hydrogen under high pressures, over 100 bar. The main constraint of the room temperature hydride compounds is the low gravimetric hydrogen storage capacities ranging from 1 to 3 wt.% H_2 , though they do have considerable hydrogen volumetric capacity of about 100 kg/m^3 . The other categories are binary and complex hydrides, where hydrogen is chemically bound. They work in a broad range of temperatures and pressures, but the most common ranges are temperatures over 100°C and pressures from 10 to 200 bar. There are some exceptions such as non-stable hydride compounds at room temperature, as for example $\text{Ti}(\text{BH}_4)_3$, $\text{Fe}(\text{BH}_4)_2$, $\text{Ni}(\text{AlH}_4)_2$, among others. Moreover, several binary and complex hydrides are not even reversible [15–20]. These hydrides show large gravimetric hydrogen storage capacities ranging from 4 to about 20 wt.% H_2 and also considerable volumetric hydrogen capacity from 100 to 150 kg/m^3 .

The chemical reaction for the hydride formation can be described as a reversible gas-solid reaction. For the sake of clarity, the most simple reaction between a solid metal ($\text{M}_{(\text{s})}$) and gas hydrogen ($\text{H}_{2(\text{g})}$) is herein explained. At certain temperature (T) and under certain pressure (P), $\text{M}_{(\text{s})}$ reacts with $\text{H}_{2(\text{g})}$ to form a hydride compound ($\text{MH}_{\text{x}(\text{s})}$) according to reaction (1):



Reaction (1) shows the overall process for the reversible formation of a hydride compound without any detail about reaction intermediates. As seen, the hydride

Hydrogen bond	Hydride compounds	Examples of hydride forming materials (hydride)	Main characteristics
Interstitial hydrogen	Room temperature hydrides	V (VH ₂), LaNi ₅ alloy (LaNi ₅ H ₆), FeTi alloy (FeTiH ₂), TiCrMo, TiVMn alloys, etc.	Form A _y B _x (y = 2 and x = 1, 2, 5); A= early transition or rare-earth metal, B= transition metal, rare-earth or alkaline metal.
Chemically bound hydrogen	Binary hydrides composed of Alkaline and alkaline rare earth	Li (LiH), Mg (MgH ₂), Na (NaH), etc.	Hydrogen is chemically bound (ionic, covalent or a mixture of both).
	Complex hydrides composed of transition metals	Mg-Fe (Mg ₂ FeH ₆), Mg ₂ Ni (Mg ₂ NiH ₄), etc.	Mg ₂ ⁺ [T _n H _n] ⁶⁻ (T = Ti, Co, Fe, among others, n= 4, 5 and 6).
	Complex hydrides containing boron (B): Borohydrides	Li-B (LiBH ₄), Ca-B (Ca(BH ₄) ₂), etc.	[BH ₄] ⁻ M ⁺ (M= alkaline, earth-alkaline, transition, rare-earth metal).
	Complex hydrides containing aluminum (Al): Alanates	Li-Al (LiAlH ₄), Na-Al (NaAlH ₄), etc.	[AlH ₄] ⁻ M ⁺ (M= alkaline, earth-alkaline, transition, rare-earth metal).
	Complex hydrides containing nitrogen (N): Amides	Li-N (LiNH ₂), Mg(NH ₂) ₂ , etc.	[NH ₂] ⁻ M ⁺ (M= alkaline, earth-alkaline, transition, rare-earth metal).

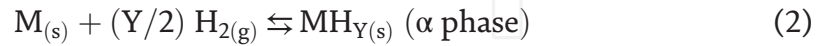
Table 1.
General classification of hydride compounds and their main characteristics [15–20].

compound formation is exothermic, while its decomposition is endothermic. Moreover, the formation and decomposition of a hydride compound occur under certain T and P conditions, which depend on the kind of M_(s) and the resulting hydride compound. Thus, these T and P conditions are determined by the thermodynamics and kinetics of the metal-hydrogen (M-H₂) system.

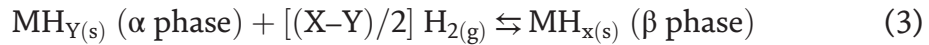
2.2 Thermodynamics

Thermodynamic properties for the M-H₂ systems are usually characterized by measuring pressure-composition-isotherms (PCIs). **Figure 3A** shows ideal PCIs (without slope and hysteresis), where the x-axis is the hydrogen concentration (C_H) expressed as the ratio between atomic hydrogen and metal (H/M), and y-axis is the hydrogen pressure (pH₂). The procedure to measure a PCI consist in introducing the hydride forming metal or material in a sealed vessel connected to hydrogen supply and increase steeply the hydrogen pressure at a constant temperature. There are different steps involved during the hydrogen absorption process in a metal under equilibrium conditions. For example, taking the PCI at T₂ (**Figure 3A**), a detailed description of the process during PCI characterization can be done as follows [4, 21]:

1. At the beginning of the process, molecular hydrogen (H_2) near the metal's surface suffers van der Waals interactions. This H_2 -M interaction process is called physisorption.
2. Molecular H_2 dissociates on the metal's surface ($H_2 \rightarrow H + H$) and forms a M-H bond. This process is called chemisorption and the required energy for it depends on the elements on the metal's surface.
3. Chemisorbed H diffuses to the interstitial site of the metal's lattice and exothermically dissolves to form a solid solution (α phase). This process occurs in the low hydrogen concentration zone ($H/M < 0.1$), as shown in **Figure 3A**—point (a) and is described by reaction (2):



4. Increasing the hydrogen pressure, the solid solution (α phase) reaches a hydrogen saturation concentration at $H/M = 0.1$. From this hydrogen concentration, the hydride phase (β phase) starts to form as shown in **Figure 3A**—point (b). Significant expansions of the metal's lattice causes strong H-H interactions which result in the nucleation and then further growth of the hydride phase. In an ideal case, the overall process of formation of the hydride phase occurs under constant pressure and is called plateau region in the PCI curve, **Figure 3A**—from point (b) to point (d). In this region, the solid solution (α phase) and the hydride phase (β phase) co-exist in equilibrium conditions, **Figure 3A**—point (c). The pressure associated to the plateau region is called equilibrium pressure ($P_{eq.}$). Reaction (3) describes the process:



5. Once the formation of the hydride phase is finished, the hydrogen pressure increases again, as shown in **Figure 3A**—from point (d). This phenomenon is ascribed to the atomic hydrogen dissolution in the hydride phase.

Under experimental conditions, the equilibrium pressure during the “plateau region” is not perfectly constant, as shown in **Figure 3C**. The sloppy plateau is attributed to expansions of the lattice of the hydride and relaxations of the metallic matrix, which causes a slight increase of the equilibrium pressure during the chemical reaction of the hydride phase (β phase) formation. Furthermore, it is also observed in

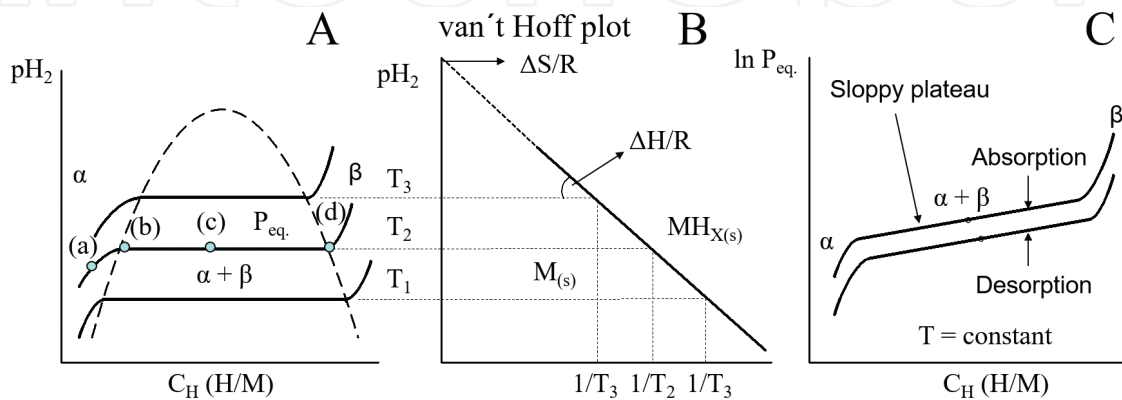


Figure 3. (A) Ideal PCIs for the description of the hydrogen absorption-desorption process through hydride compound formation in equilibrium conditions. (B) van't Hoff plot built from PCIs. (C) PCIs showing the real behavior with slope and hysteresis.

Figure 3C that the equilibrium pressure for the hydrogenation process is lower than the equilibrium pressure for the dehydrogenation process. This phenomenon is called hysteresis and it is ascribed to localized defects in the metallic lattice and inhomogeneity on the metal's surface [21–23]. Therefore, different equilibrium pressures for the hydrogenation and dehydrogenation processes are usually reported.

The dependence of the equilibrium pressure (P_{eq}) on the temperature (T) is given by the van't Hoff Eq. (4):

$$\ln P_{eq} = \left[\frac{\Delta H}{RT} \right] - \left[\frac{\Delta S}{R} \right], \tag{4}$$

where ΔH and ΔS are the enthalpy and entropy changes for the chemical reaction of the hydride phase formation, respectively, and R is the ideal gas constant. Values for ΔH and ΔS can be obtained from the slope and intercept of the linear correlation between the $\ln(P_{eq})$ and $1/T$, as shown in **Figure 3B**. This linear correlation is built from the equilibrium pressures determined by the PCI measurements (pH_2 during the plateau region—**Figure 3A**—from point (b) to point (d)) at each temperature (T_1 , T_2 , etc.). ΔS indicates the entropy change for hydrogen, i.e., from molecular gas hydrogen to hydrogen in the hydride phase. For metal-hydrogen systems, the standard entropy change for hydrogen is 130 kJ/K mol, but it can have a different value for other kind of hydride systems as for example for hydrides composed of boron, aluminum, or nitrogen and alkaline or alkaline earth metals [4, 21]. ΔH of the hydride compound or system characterizes the stability of the metal-hydrogen bond (M–H) and it takes a negative value for the exothermic hydrogenation and a positive value for the endothermic dehydrogenation. These two thermodynamic parameters, i.e., ΔH and ΔS , are quite important for hydride forming material design and hence for practical applications. They allow calculating the temperature for the hydrogen release from hydride phase under atmospheric pressure (~ 1 bar), which refers to the minimum temperature for the dehydrogenation process without any kind of kinetic restriction. Additionally, the thermodynamic properties of the hydride phase provide information about the range of temperature and pressures at which the hydride system works. **Table 2** shows the experimental enthalpy, entropy values, and decomposition temperature under 1 bar

Hydride compound/ Hydride system	ΔH [kJ/mol H ₂]	ΔS [J/K mol H ₂]	$T_{decomposition} = \Delta H/\Delta S$ at 1bar [°C]	Ref.
LaNi ₅ H ₆	31.8	110.0	16	[24]
MgH ₂	74	135	275	[25]
Mg ₂ FeH ₆	80	137	311	[26]
LiBH ₄	74	115	370	[27]
⁽¹⁾ NaAlH ₄	42	124	66	[28]
LiNH ₂	45	n.a.	-	[29]
⁽²⁾ 2LiBH ₄ +MgH ₂	40.5	81.3	255	[30]
Mg(NH ₂) ₂ +2LiH	38.9	107 ⁽³⁾	90	[31]

(1) The values are reported as an average of the two steps reaction from NaH and Al to NaAlH₄ [28].
(2) Values obtained from hydrogenation PCIs, assuming one reaction step [30].
(3) Entropy calculated from the reported van't Hoff plot [31]. n.a. = not available.

Table 2.
Dehydrogenation thermodynamic parameters and decomposition temperature under 1 bar H₂ for some hydride compounds and systems.

H₂ for some hydride compounds and systems, which have been under intensive research [24–31].

Table 2 clearly indicates that the use of some hydride compounds and systems for solid-state hydrogen storage system working under mild temperature conditions is thermodynamically feasible. Moreover, other cases such as Mg₂FeH₆ are more suitable for energy storage because of its large enthalpy value. All efforts toward the design of hydride compounds, especially for mobile applications, have been focused on reaching enthalpy values ranging between 40 and 50 kJ/mol H₂, leading to an operative temperature between 20 and 90°C. It seems that some materials such as room temperature hydride fulfill these requirements, but the thermodynamic stability is not the unique parameter that determines the practical application of the hydride compound, since the capacity plays a major role. For this reason, high gravimetric hydrogen capacities are required as well, and room temperature hydrides do not meet this requirement at the time to work at low hydrogen pressure.

3. Fundamental concepts about hydrogenation-dehydrogenation kinetics

Most of the hydride compounds and hydride systems cannot work at the temperature predicted by the thermodynamics. This fact is related to kinetic constraints, leading to notable higher operative temperatures than that thermodynamically feasible. For this reason, enhancing the kinetic behavior of hydride compounds and hydride systems has been matter of intensive research. To start with a comprehensive development about the strategies to improve the kinetic behavior of the hydride compounds and systems, it is important to introduce fundamental concepts and details about the experimental method used to understand and to tailor the hydrogenation/dehydrogenation rates, respectively.

The kinetic behavior for the formation/decomposition of a hydride compound gives information about the time required for the material to uptake/release hydrogen in non-equilibrium (dynamic) conditions. **Figure 4** shows experimental kinetic hydrogenation and dehydrogenation curves for Nb₂O₅-doped MgH₂. These curves show hydrogen concentration as a function of time. For the sake of clarity, all the explanation and description is referred to a nominal metal hydride (MH_{x(s)}, M = metal, H = hydrogen). The absorbed/desorbed hydrogen concentration is expressed in terms of fraction (α), which is the ratio between the absorbed/desorbed hydrogen concentration at each time during the process and the

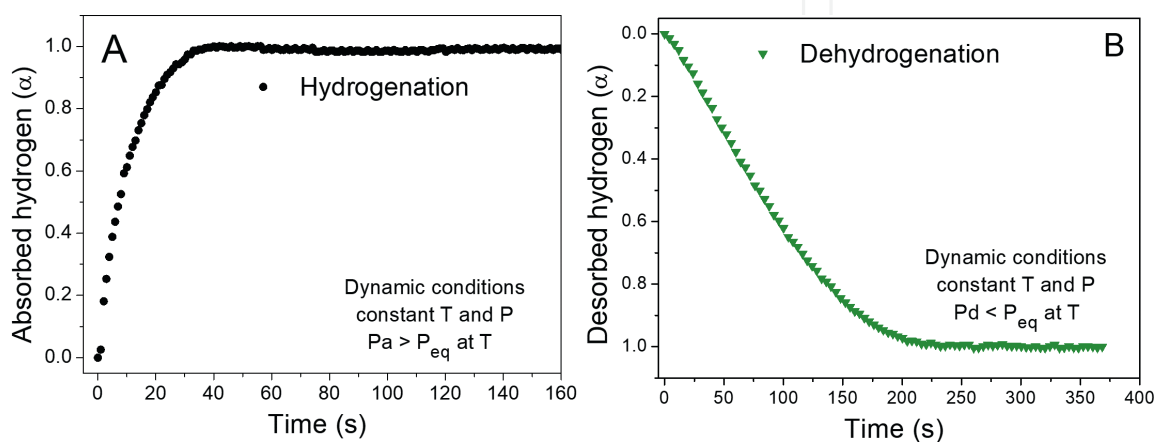


Figure 4.
(A) Hydrogenation kinetic behavior and (B) dehydrogenation kinetic behavior for metal-hydrogen system.

maximum absorbed/desorbed hydrogen concentration. Under dynamic conditions, the hydrogenation reaction happens when the operative pressure (P_a) is over the equilibrium pressure (P_{eq}) of the hydride phase at the operative temperature (T), **Figure 4A**. On the contrary, for dehydrogenation under dynamic conditions, the operative pressure (P_d) has to be below the equilibrium pressure (P_{eq}) of the hydride phase at the operative temperature (T), **Figure 4B**. The procedure to measure a kinetic curve for the hydrogenation/dehydrogenation consist in introducing the hydride forming metal or material in a sealed vessel connected to hydrogen supply and suddenly increase/decrease the hydrogen pressure at a constant temperature, respectively. After the sudden pressure increase/decrease, the operative pressure is kept constant and higher/lower than the P_{eq} for the hydrogenation/dehydrogenation dynamic processes, respectively. The measurement of the kinetic curve runs until reaching saturation, i.e., $\alpha = 1$.

In order to clarify the complexity of the hydrogenation/dehydrogenation processes under dynamic conditions, the sequence of involving steps can be simply described as follows:

3.1 Hydrogenation process

- a. **Physisorption:** The hydrogen molecule approaches to the metal and interacts with the metal's surface through van der Waals forces.
- b. **Chemisorption:** On the metal's surface, the hydrogen molecules dissociate and the atomic hydrogen forms chemical bonds with the metal.
- c. **Penetration through the α phase surface:** Hydrogen atoms penetrate the metal's surface.
- d. **Hydrogenation:** Formation of the β phase (hydride phase).
- e. **Diffusion through the β phase:** Hydrogen atoms diffuse through the β phase (hydride phase).
- f. **Nucleation and growth:** The β phase (hydride phase) starts to nucleate and grows with α/β interface movement.

The **dehydrogenation process** proceeds in the opposite way, as described above. In **Figure 5**, the involved steps during the hydrogenation and dehydrogenation processes in dynamic conditions are shown.

In the previous description (**Figure 5**), any fluid dynamic and heat transfer restrictions associated to large amounts of material are not taken into account. For instance, fluid dynamic restriction occurs when hydrogen can flow into the material's bed. For the case of the heat transfer restrictions, it is referred to the notable temperature increase or decrease during the exothermic or endothermic hydrogenation or dehydrogenation reaction, respectively. The heat transfer through the hydride bed is not efficient because the thermal conductivity of the hydride compounds is rather low. For these reasons, the analysis on the kinetic behavior and tailoring will be performed for a punctual mass of hydride bed without any fluid dynamic and heat transfer restriction.

There are functional dependences of the hydrogenation/dehydrogenation reaction rates on the temperature, pressure, and morphology of the material. The rates for gas-solid reactions, such as the ones occurring during the hydride formation and decomposition, can be described by Eq. (5) [32, 33]:

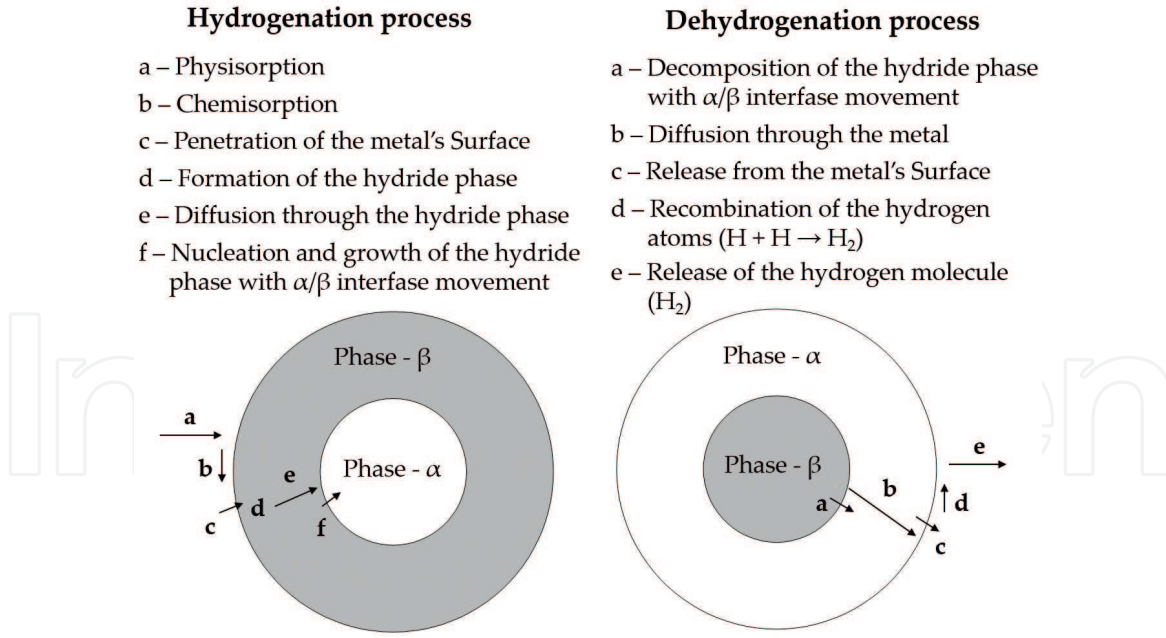


Figure 5.
Steps involved in the hydrogenation and dehydrogenation processes under dynamic conditions.

$$\frac{d\alpha}{dt} = K(T) \times F(P) \times G(\alpha), \quad (5)$$

where the overall reaction rate, $d\alpha/dt$ (α = hydrogen fraction and t = time) is function of the temperature, $K(T)$, of the pressure, $F(P)$, and of the intrinsic and morphological changes of the material occurring during the hydrogenation/dehydrogenation process, $G(\alpha)$, which is function of the hydrogen fraction (α). As shown by Eq. (5), the dependencies of the rate on the $K(T)$, $F(P)$, and $G(\alpha)$ can be investigated independently by keeping two of them constant. In the following sections, each dependence will be explained.

3.2 Dependence on the intrinsic and morphological changes of the material $G(\alpha)$

At constant temperature and pressure, the reaction rate depends on intrinsic factors and morphological changes of the solid (defects, crystalline structure, size and morphology of the particles, etc.), i.e., $G(\alpha)$ [34, 35]. Thus, Eq. (5) can be expressed:

$$\frac{d\alpha}{dt} = k \times G(\alpha) \quad (6)$$

$$k = K(T) \times F(P), \quad (7)$$

k is the kinetic constant and it contains the temperature and pressure dependences as seen in Eq. (7). Reordering Eq. (6), it is possible to obtain an expression for the evaluation of $G(\alpha)$:

$$g(\alpha) = \int_0^\alpha \frac{d\alpha}{G(\alpha)} = k \times t, \quad (8)$$

where $g(\alpha)$ is the integral form of the gas-solid kinetic models for the material's changes. The gas-solid kinetic models describe different physical phenomena. There are four main sets of models: (1) nucleation and growth models, (2) geometrical

contracting models, (3) diffusion models, and (4) autocatalytic models. In **Table 3**, the integral form of the gas-solid kinetic models is described. There are more gas-solid models, but it is not the aim to perform exhaustive description of them.

Among the steps involved in the hydrogenation/dehydrogenation processes (**Figure 5**), it is usually found a slowest one, which limits the overall reaction rate of the process. Thus, the slowest step is commonly called “rate-limiting step.” The determination of the rate-limiting step depends on the kind of hydride and the experimental conditions. Identifying the rate-limiting step requires the application of gas-solid models shown in **Table 3**. The determination of the rate-limiting step is carried out by measuring kinetic curves under constant temperature and pressure, as the ones shown in **Figure 4**. Once, the hydrogen uptake and release against time is expressed in terms of hydrogen fraction, α , the integral models can be applied to build a graph of $g(\alpha)$ as function of time.

A first approach to study which process limits the hydrogenation/dehydrogenation kinetic behavior is to find which model has the best linear fitting of the integral

Model	Description	Integral form $g(\alpha) = k \times t$
Nucleation and growth models		
Johnson-Mehl-Avrami (JAM), $n= 1$	One-dimensional growth with interface-controlled reaction rate	$[-\ln(1 - \alpha)]^{1/n}$
Johnson-Mehl-Avrami (JAM), $n= 2$	Two-dimensional growth of existent nuclei at constant interface rate	
Johnson-Mehl-Avrami (JAM), $n= 3$	Three-dimensional growth of existent nuclei at constant interface rate	
Johnson-Mehl-Avrami (JAM), $n= 1.5$	Three-dimensional growth of random nuclei with decreasing interface rate, diffusion controlled	
Geometrical contracting models		
Contracting area (CA), $n= 2$	Two-dimensional growth of contracting volume with constant interface rate	$1 - (1 - \alpha)^{1/n}$
Contracting volume (CV), $n= 3$	Three-dimensional growth of contracting volume with constant interface rate	
Diffusion models		
1-D Diffusion	Surface control (Chemisorption)	α^2
2-D Diffusion	Two-dimensional diffusion controlled growth with decreasing interface rate	$[(1 - \alpha)\ln(1 - \alpha)] + \alpha$
3-D Diffusion	Three-dimensional diffusion controlled growth with decreasing interface rate	$1 - \left(\frac{2}{3}\right)\alpha - (1 - \alpha)^{2/3}$
Autocatalytic models		
Modified Prout-Tompkins	Acceleration of the reaction rate with product (s) generation. $a =$ constant	$\ln \left[\frac{a}{(1 - a)} \right]$

Table 3.
Integral form of the gas-solid models [32, 33, 36].

form, $g(\alpha)$, of the solid-state models against time. First, the hydrogen fraction range considered for the fitting is usually from 0.1 to 0.9. On one hand, at the beginning of the process the initial points involve a high degree of uncertainty, mainly for fast rates in the range of seconds. On the other hand, the final stage of the process, reaching the saturation of the material, does not play any role in the determination of the rate-limiting step. As an example, **Figure 6** exhibits $g(\alpha)$ generated from each model, **Table 3**, as a function of time in the range of α between 0.10 and 0.90 for the hydrogenation and dehydrogenation process shown in **Figure 4**. Then, a linear fitting was performed in each curve.

As seen, the simple linear fitting of the integral form of the solid state-models does not provide a clear clue about the rate-limiting step for the hydrogenation and dehydrogenation rates. There are several models with suitable fitting goodness (highlighted in bold). For these reason, it is possible to apply other procedure such as the reduced time method proposed by Sharp and Jones [37, 38]. By applying this method, a plot for the theoretical reduced time $(t/t_{0.5})_{\text{theoretical}}$ as a function of the experimental reduced time $(t/t_{0.5})_{\text{experimental}}$ is built as shown in **Figure 7**. The $(t/t_{0.5})_{\text{theoretical}}$ is obtained by expressing the equation of the integral form of solid-state models in terms of the time at $\alpha = 0.5$, i.e., $t_{0.5}$. As an example, for the case of the integral form of the solid-gas model JMA with $n = 1$, the $(t/t_{0.5})_{\text{theoretical}}$ is obtained as follows:

$$[-\ln(1 - \alpha)] = k \times t \quad (9)$$

$$[-\ln(1 - 0.5)] = k \times t_{0.5} \quad (10)$$

The right term of Eq. (10) is equal to 0.69. Replacing 0.69 in Eq. (10) and dividing (9) over (10), Eq. (11) provides the $(t/t_{0.5})_{\text{theoretical}}$

$$\frac{[-\ln(1 - \alpha)]}{0.69} = \left[\frac{t}{t_{0.5}} \right]_{\text{theoretical}} \quad (11)$$

The $(t/t_{0.5})_{\text{experimental}}$ is directly obtained from the experimental results, **Figure 4**, by dividing the time during the measurement (t) over the time at $\alpha = 0.5$. The rate-limiting step is determined by three parameters, i.e., the fitting goodness, slope, and intercept of the linear fitting. This represents an advantage in comparison with the simple linear fitting of the integral form of the solid-state models, with just the fitting goodness as one decision parameter. The best fitting obtained from

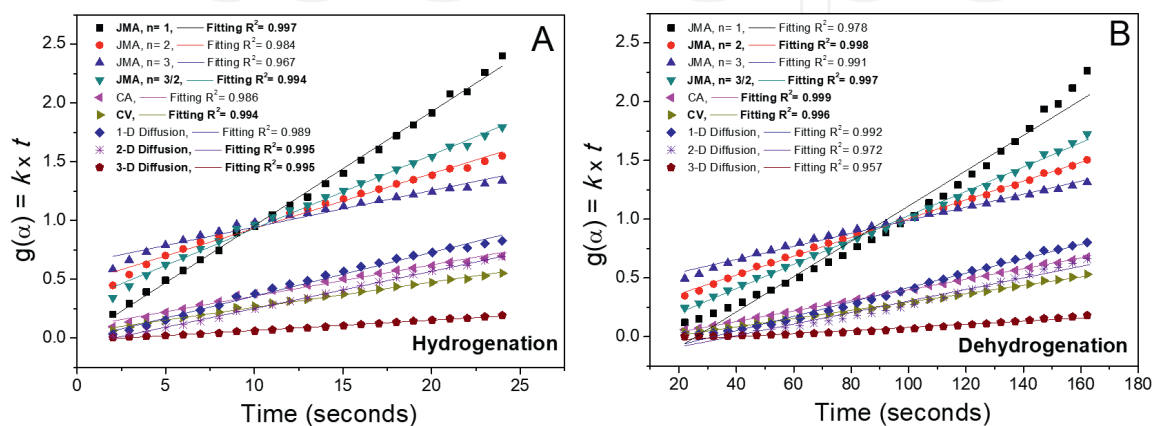


Figure 6. Application and fitting of the integral form of the solid-state models (**Table 3**) to the hydrogenation/dehydrogenation rates shown in **Figure 4**.

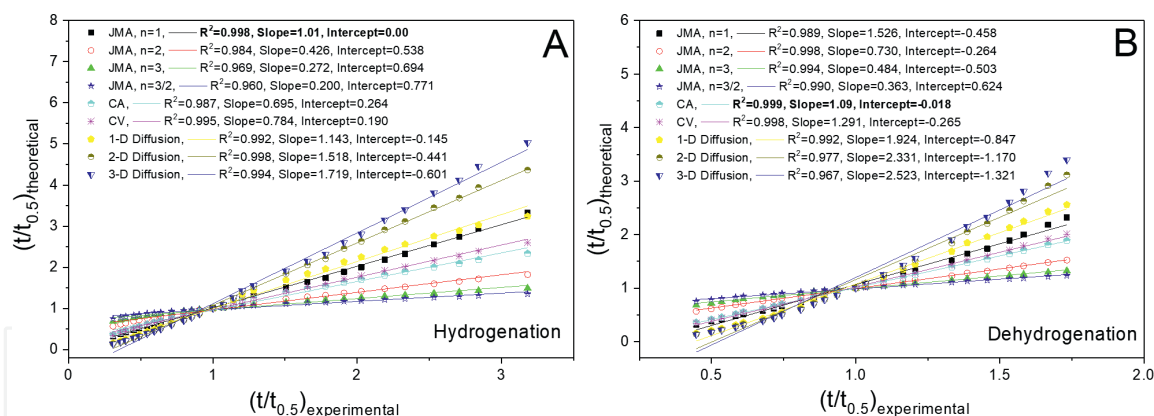


Figure 7. Reduced time method: Plots $(t/t_{0.5})_{\text{theoretical}}$ vs. $(t/t_{0.5})_{\text{experimental}}$ and fitting for (A) hydrogenation and (B) dehydrogenation rates.

the reduced time method is the one showing linear fitting goodness and slope equal to 1 and intercept equal to 0.

Figure 7 shows that for the case of the hydrogenation rate the model JMA, $n = 1$, **Table 3**, provides the best linear fitting (slope = 1, intercept = 0 and goodness ≈ 1). For this reason, the overall reaction rate is limited by one-dimensional growth with interface-controlled reaction rate. This rate-limiting step is related to the step (f) described in **Figure 5**. For the dehydrogenation rate, the rate-limiting step is the two-dimensional growth of contracting volume with constant interface rate (CA), related to the step (a) shown in **Figure 5**.

In fact, the kinetic analysis based on the solid-state models should be also based on additional experimental evidence obtained from the material science characterizations for morphological and microstructural changes before and after and upon hydrogenation and dehydrogenation kinetic processes.

3.3 Temperature dependence $K(T)$

Under constant pressure, the hydrogenation/dehydrogenation reactions speed up as the temperature increases and this temperature dependence is described by the Arrhenius expression. The dependence of the hydrogenation/dehydrogenation reaction rates on the temperature follows Eq. (12):

$$K(T) = A \times \exp(-E_a/RT), \quad (12)$$

where A is the pre-exponential factor or frequency factor and represents the frequency of collisions between reactant molecules, E_a is the apparent activation energy, which is the energy required to start the reaction, R is the gas constant, and T is the absolute temperature.

The activation energy is a relevant kinetic parameter to evaluate the kinetic performance of a hydride forming material. Isothermal and non-isothermal measurements can be performed to obtain the activation energy. Two procedures are commonly used. The first consists in performing isothermal measurements at different temperature and constant pressure, such as the ones shown in **Figure 4**. Then, by the application of the gas-solid models, it is possible to calculate the kinetic constant “ k ,” once identified the rate-limiting step as explained in Section 3.1. As expressed in Eq. (7), k depends on $K(T)$ and $F(P)$. Considering isobaric measurements, k is only function of $K(T)$ following the Arrhenius expression:

$$k = A \times \exp(-E_a/RT), \quad (13)$$

Applying natural logarithm to Eq. (13):

$$\ln k = \ln A + \ln(-E_a/RT) \quad (14)$$

Plotting $\ln k$ against $1/T$, the slope of the linear fitting provides the E_a in kJ/mol H_2 and the intercept the frequency factor A , as seen in **Figure 8A**. The second method involves non-isothermal measurements done via calorimetric methods such as scanning differential calorimetry (DSC) and differential temperature analysis (DTA) [39]. This method is the Kissinger one [40]. The method consists in determining temperature maxima (T_m) of the exothermal (hydrogenation)/endothermal (dehydrogenation) events obtained from the DSC or DTA measurements at different constant heating rate (ϕ). The change of T_m with ϕ is directly related to the nature of the reaction.

At a constant heating rate (ϕ), constant pressure (P) and considering k has an Arrhenius dependence on the temperature, Eq. (13), Eq. (5) can be expressed:

$$\frac{d\alpha}{dt} = \frac{A}{dt} \times \exp(-E_a/RT) \times G(\alpha) \quad (15)$$

Assuming that the fraction at the peak maximum and $G(\alpha)$ are independent on ϕ , reordering and applying natural logarithm to expression (15), it is possible to write:

$$\ln \left[\frac{\phi}{T_m^2} \right] = -\frac{E_a}{RT_m} + \ln \left[\frac{AR}{E_a} \right] + C \quad (16)$$

Figure 8B shows the DSC curves at different ϕ for a dehydrogenation process, from which the peak maxima are selected. Then, a plot of the $\ln(\phi/T_m^2)$ against $1/T$ is built and the E_a in kJ/mol H_2 is obtained from the slope of the linear fitting, as shown in **Figure 8C**.

Table 4 shows examples for experimental activation energy (E_a) values, reaction mechanism, and rate-limiting steps for different materials. As seen, the lowest E_a values are related to surface controlled process such as physisorption and chemisorption (**Figure 5**: Hydrogenation process—Steps **a** and **b** and Dehydrogenation process—Steps **d** and **e**). On the contrary, bulk processes such as interface controlled and diffusion processes present higher E_a values (**Figure 5**: Hydrogenation process—Steps **c**, **e**, and **f** and Dehydrogenation process—Steps **a** and **b**). The

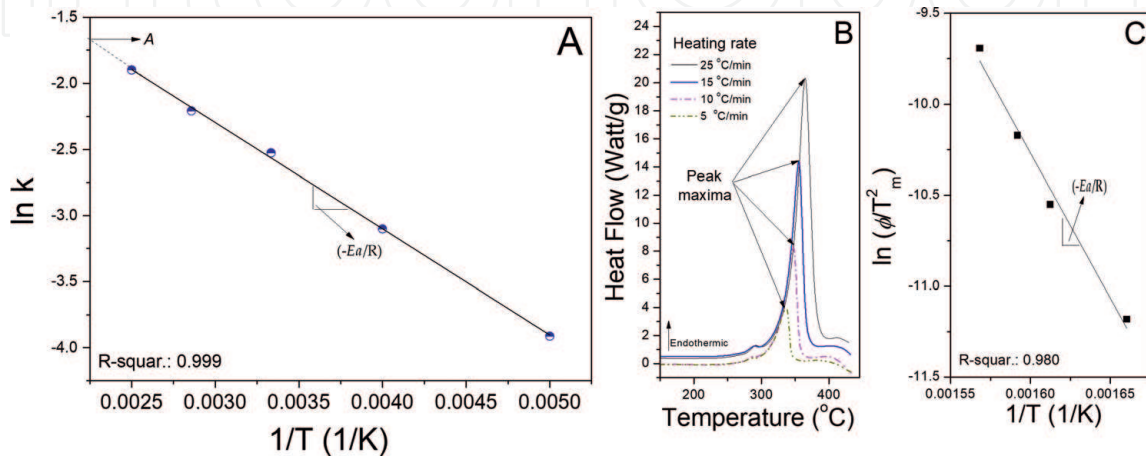


Figure 8. Activation energy determination: (A) isothermal method, (B) DSC curves for the (C) non-isothermal method.

Ea [kJ/mol H ₂]	Process, material, physical meaning,rate-limiting step	Ref.
54.1	Dehydrogenation for LaNi _{4.7} Al _{0.3} -H. Rate limiting step: Nucleation and Growth ($\alpha+\beta$ phases).	[41]
28.9	Dehydrogenation for LaNi ₅ . Rate-limiting step: Surface control and chemical reaction.	[42]
40 \pm 2	Dehydrogenation LaNi ₅ H _x . Shrinking core model. Rate-limiting step: Controlled interface reaction at the β/α interface.	[43]
9.1	Hydrogenation for LaNi ₅ . Rate-limiting step: Surface control. H ₂ molecule dissociation on the surface of the β phase (high temperature)	[44]
45.5	Hydrogenation for LaNi ₅ . Rate-limiting step: Bulk diffusion control. Diffusion of hydrogen atoms through the β phase (low temperature)	
19	Hydrogenation for Ti _{0.98} Zr _{0.02} V _{0.43} Fe _{0.09} Cr _{0.05} . Rate limiting step: Diffusion of hydrogen atoms.	[45]
62	Dehydrogenation for Mg ₂ Ni. Rate-limiting step: Diffusion of hydrogen through the α phase.	[46]
12.8	Dehydrogenation for MnNi _{4.5} Al _{0.5} . Rate-limiting step: Chemisorption on the active sites and α/β interface.	[47]
46.5	Hydrogenation for MnNi _{4.5} Al _{0.5} . Rate-limiting step: Hydrogen diffusion through the hydride (β) phase.	
39.9	Hydrogenation for LaNi ₅ . Rate-limiting step: Hydrogen diffusion through the hydride (β) phase.	[48]
33.0	Hydrogenation for LaNi ₅ . Rate-limiting step: Controlled interface reaction at the β/α interface.	[49]
0.92	Hydrogenation for Mg ₂ Ni. Dissociative chemisorption of the H ₂ molecule. Segregated and excess nickel as active sites for dissociation.	[50]
90 \pm 10	Hydrogenation for Mg/MgH ₂ . Rate-limiting step: Nucleation and growth mechanism for the β phase.	[51]
100 \pm 10	Dehydrogenation for MgH ₂ . Rate-limiting step: hydrogen diffusion through the β phase. Corrected by $F(P)$	
160 \pm 10	Hydrogenation of 2LiH+MgB ₂ +0.05molTiCl ₃ . Rate limiting step: One-dimensional interface controlled. Corrected by $F(P)$.	[52]
350 \pm 10/238 \pm 4	Dehydrogenation for 2LiBH ₄ +MgH ₂ +0.05molTiCl ₃ . First step: dehydrogenation of MgH ₂ /Second step: Dehydrogenation of LiBH ₄	

Table 4.
Activation energies, reaction mechanisms, and rate-limiting steps.

interface and diffusion controlled processes are the most common ones for the hydride compounds formation/decomposition [41–51].

It is important to point out that the isothermal method for Ea requires the knowledge of the rate-limiting step, thus it depends on the solid-state model. On the contrary, the non-isothermal method is independent on the solid-state model, which represents an advantage over the first method. However, for the kinetic modeling of the reaction rates, as indicated by Eq. (5), the determination of $G(\alpha)$ is demanding. For this reason, at the time proceed with kinetic modeling, or just determine Ea via measurements of the hydrogenation or dehydrogenation rates at isothermal conditions, it is necessary to work far away from the equilibrium pressures to avoid the effects of the driving force, i.e., the $F(P)$. In fact, rightly speaking, the $K(T)$ must be corrected by the effects of the driving force by determining $F(P)$, since the Ea values obtained after the correction are different from the one without; as an example we can mention the works published by Fenández et al. [51] and Jepsen et al. [52]. In the next subsection, then, the $F(P)$ dependency is described.

3.4 Pressure dependence $F(P)$

At constant temperature, the hydrogenation/dehydrogenation reactions show a dependence on a functional relationship between the operative pressure (P) and the equilibrium pressure (P_{eq}) for both hydrogenation and dehydrogenation processes. This dependence is called $F(P)$. **Table 5** describes the most relevant $F(P)$ applied to different materials and their physical meaning. These functions were obtained from experimental investigations and proposed in pioneering works about the kinetic

$F(P)$	Physical meaning / rate-limiting step / material	Ref.
$(P/P_{eq})^n$, $n=1$	$F(P)$ developed considering the reversible nature of the hydrogenation/dehydrogenation reactions in $\text{LaNi}_{4.7}\text{Al}_{0.3}$ alloy. Rate-limiting step: Nucleation and growth in the $\alpha+\beta$ phase.	[41]
$(P - P_{eq})/P_0$	Chemical reaction as rate-limiting step. It was determined for the dehydrogenation reaction of LaNi_5H_x as the best-fitted function. $P_0 = 1$ bar (reference pressure).	[42]
$\ln(P/P_{eq})$	$(\beta)\text{LaNi}_5\text{H}_6 \rightarrow (\alpha)\text{LaNi}_5\text{H}_x + (3-x/2)\text{H}_2$: Isothermal dehydrogenation. Shrinking core model, with interphase controlled as rate-limiting step, assuming that the surface is perfectly porous, so that neither diffusion nor mass transport can be rate-limiting steps. Therefore, the chemical potential acts across the β/α interface.	[43]
	Hydrogenation of LaNi_5 : Diffusion of H atoms from the surface through the growing β phase to the α/β interface.	
$(P_{eq} - P)$	Dehydrogenation of LaNi_5 : Surface controlled as rate-limiting step (Recombination of the H_2 molecule on the α surface).	[44]
$P^{0.5}$	Hydrogenation for $\text{Ti}_{0.98}\text{Zr}_{0.02}\text{V}_{0.43}\text{Fe}_{0.09}\text{Cr}_{0.05}$. Diffusion of H-Atom as rate-limiting step.	[45]
$(P_{eq}^{0.5} - P^{0.5})$	Dehydrogenation for the Mg_2Ni alloy (Mg_2NiH_4). Rate-limiting step: Diffusion of hydrogen through the α phase at low and high pressures.	[46]
$(P - P_{eq})$	Hydrogenation for $\text{MnNi}_{4.5}\text{Al}_{0.5}$. Rate-limiting step: Chemisorption on the active sites and α/β interface.	[47]
$(P^{0.5} - P_{eq}^{0.5})$	Hydrogenation for $\text{MnNi}_{4.5}\text{Al}_{0.5}$. Rate-limiting step: Hydrogen diffusion through the hydride phase.	
$(P - P_{eq})$	Hydrogenation for Mg_2Ni . Rate-limiting step: Dissociative chemisorption of the H_2 molecule.	[50]
$(1 - P/P_{eq})^2$	Hydrogenation for Mg/MgH_2 . Nucleation and growth process. Rate-limiting step: JMA with n between 0.5 to 1	[51]
P	At room temperature, the pressure dependence of the H_2 reaction on Ti surfaces contaminated with CH_4 , CO , CO_2 , H_2O , O_2 , N_2 and SO_2 is approximately proportional to P (operative pressure).	[53]
$(P_{eq} - P_v)/P_{eq}$	$\text{TiFe}_{0.8}\text{Ni}_{0.2}$: Investigations on kinetics after prolonged cycling. No physical meaning. P_v : instantaneous differential pressure in the collecting desorption reservoir.	[54]
$1 - (P/P_{eq})^{0.5}$	Hydrogenation for Mg/MgH_2 . Rate-limiting step: Diffusion	[55]

Table 5.
Pressure dependencies, their physical meaning, and rate-limiting step.

behavior of hydride compounds [41–47, 50, 51, 53–55]. Moreover, the shown $F(P)$ were also applied to characterize the kinetic behavior and to model the reaction rates of different hydride compounds and hydride systems; exemplary for NaAlH_4 complex hydride with Ti-based catalyst [56, 57]. As seen, the developed $F(P)$ depends on the hydride forming material and each $F(P)$ is associated to different rate-limiting step and physical meaning. It is important to mention that the experimental conditions also play a major role for the pressure dependence, thus it is possible to find works in which the same material was investigated, but the pressure dependences are different, and this fact is mainly related to different experimental setups.

In this section, all the basics concepts for the right understanding of the kinetic behavior of the hydride compounds and dependencies of the hydrogenation/dehydrogenation reaction rates were exposed. Now, it is possible to describe the main strategies applied to improve the hydrogenation/dehydrogenation rates for some hydride compounds and hydride systems under extensive research.

4. Strategies to tailor the kinetic behavior of hydride compounds and systems

Investigations on the kinetic tailoring to improve the hydrogen storage properties of hydride compounds and hydride systems involve knowledge about the thermodynamic behavior and kinetic behavior of the hydride system. First, equilibrium pressures at different temperatures are needed to plan the experimental pressure and temperature for the characterization of the kinetic behavior. Second, some knowledge about the mechanism(s) that constraint the overall reaction rates is also required. For this reason, it is important to know or at least have clues about possible rate-limiting steps for the hydrogenation/dehydrogenation processes, as well as the influence of the temperature and pressure dependences on the reaction rates. In this regard, knowledge about $K(T)$ allows quantifying in terms of E_a the effects of a tailoring strategy. In this line, knowledge of $F(P)$ dependence is usually necessary to properly determine $K(T)$. All these understanding about the thermodynamics and kinetics of the hydride compound or system matter of investigation enormously contribute to seek the best strategy to improve its hydrogenation/dehydrogenation reaction rates. Of course, there are several opportunities in which kinetic improvements for a hydride compound or system are proposed based just on a simple experimental procedure; without any previous systematic study about the thermodynamics and kinetics. This approach is also possible, but it leads to a superficial knowledge about the actual kinetic improvement and to a poor understanding of the behavior of the hydride compound or system.

The most relevant approaches to enhance the kinetic behavior of hydride compounds and systems are: (1) improving the microstructural refinement via mechanical milling, (2) doping with transition metal and transition metal compounds, (3) forming in situ catalyst, and (4) nanoconfinement. In this section, the concepts of these strategies are explained and examples for their practical application to hydride compounds and systems are also described [58–96].

In general, two or three of these strategies are applied together, as for example mechanical milling, transition metal, or transition metal compound addition and in situ catalyst formation or nanoconfinement and transition metal or compound addition, etc. However, it is possible to put emphasis on the each strategy in order to understand what the specific effects are on the hydride forming, regardless the combined application of them.

4.1 Mechanical milling

The mechanical milling process is a powder processing method. This processing technique allows producing homogeneous materials starting from powder mixtures [58]. Moreover, the mechanical milling causes particle and grain size reduction (microstructural refinement). Furthermore, mechanical milling is also applied for the synthesis of hydrides, i.e., mechanochemical synthesis [59]. This process can be carried out at laboratory scale and at industrial scale. Herein, the laboratory scale milling process of hydride compounds and systems are discussed. In general, the milling process for improving the microstructural characteristics of hydrides is performed with amounts of material ranging between 1 and 20 g. The milling vessels are usually made of stainless steel and with a volume between 50 and 250 cm³. As grinding medium stainless steel balls are used. There are several laboratory milling devices that can be classified by the injected shock power per unit mass of grinding medium (Pg), which is a parameter that determines the reached microstructural refinement of a material (powder) subjected to milling procedure. Indeed, the reached degree of microstructural refinements also depends on the milling time and the numbers of ball (grinding medium), which are parameters that can be changed at the time to perform the milling process. Among the most commonly utilized mill devices for hydride compounds and system preparation at laboratory scale, it is possible to mention: (1) Magneto Uni-ball mill device (low energy, Pg: 0.0003–0.002 W/g), (2) Planetary Fritsch-P6 (middle energy, Pg: 0.01–0.22 W/g), and Vibratory Spex 8000 M mill device (high energy, Pg < 0.24 W/g) [60, 61]. Owing to the pyrophoric nature of the hydride compounds and their easiness to get hydrolyzed and/or oxidized, the milling process is done under inert atmosphere or hydrogen atmosphere in the case of mechanochemical synthesis. The effects of mechanical milling on the material are: (1) creation of grain boundaries and defects, (2) higher degree of microstructural refinement, and (3) intimate mixture of powders. In this regard, the first two effects improve the activation process of the material for the initial hydrogen absorption and the hydrogenation/dehydrogenation kinetic processes due to the enhancement of hydrogen diffusion through new pathways and shorter distances. Grain boundaries and defects are created by the mechanical energy provided during the milling process. More grain boundaries provide larger surface area and shorter diffusion distance for hydrogen, while the presence of defects acts as channels for hydrogen diffusion. Both effects ease the contact between hydrogen and fresh hydride forming material, enhancing the kinetic behavior. The third effect contributes to the homogeneous distribution and intermixture of the main components of the material and an additive. Moreover, the milling process can promote interactions between the main components and the additive, leading to the formation of other species with favorable effects on the kinetic behavior. This effect will be addressed in a following section. **Figure 9** shows the effects of mechanical milling under hydrogen (0.5 bar) atmosphere for 150 h on a mixture of Mg + 10 wt.%Fe in a Magneto Uni-ball mill device. As seen in the SEM photos (Scanning Electron Microscopy), the particle sizes are notably reduced and the surface has porous characteristic in comparison to the starting material. These results account for the mechanical effects of the milling process as well as the fragilization of Mg (ductile material) because of the *in situ* formation of MgH₂ (brittle material) under H₂ atmosphere. The effects of milling on Mg + 10 wt.%Fe markedly improve its kinetic behavior by reducing the diffusion pathways for the hydrogen absorption [62].

In 1997, Zaluska et al. [63] reported a pioneering work about the properties of different as-milled hydride forming materials such as Mg, Mg₂Ni, FeTi, and LaNi₅. It was found that the materials after milling presented a nanocrystalline nature,

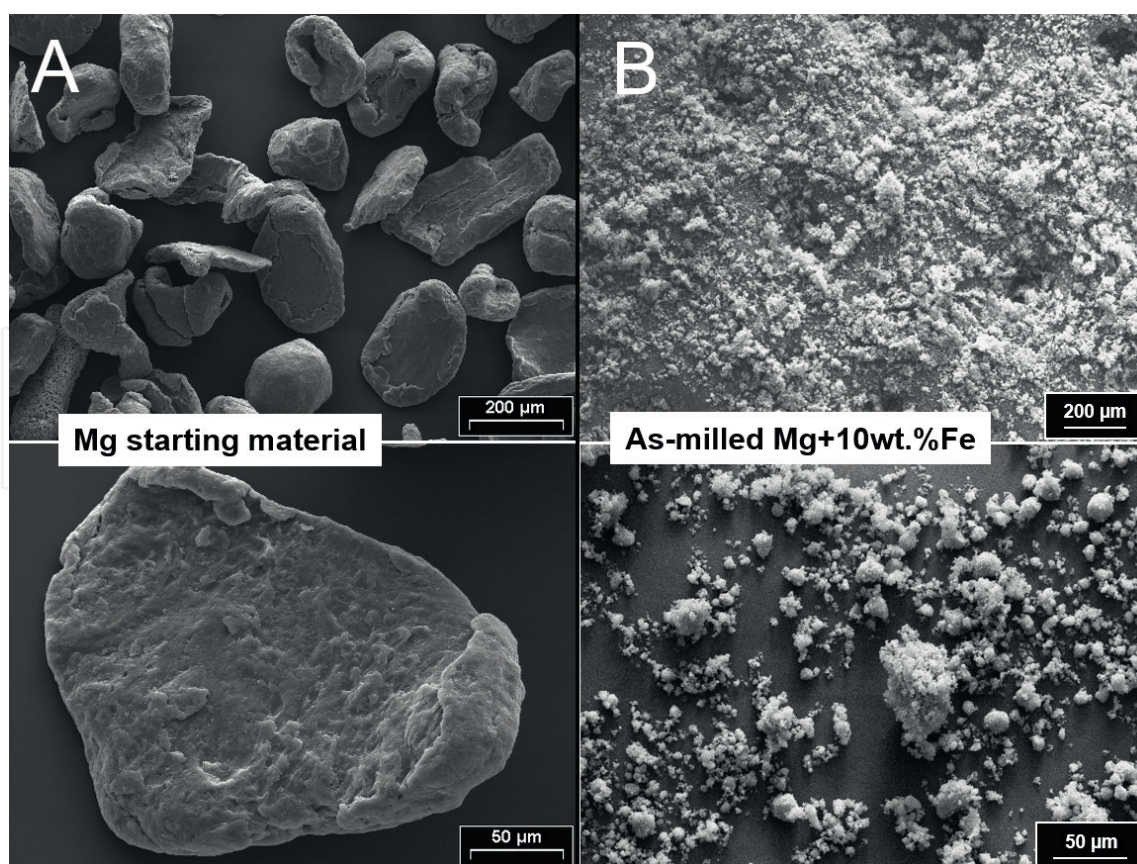


Figure 9.
SEM photos for (A) Mg starting material and (B) Mg + 10 wt.%Fe after 150 h of milling under 0.5 bar H_2 in a magneto Uni-ball device.

causing notable improvements in the hydrogenation/dehydrogenation kinetic behavior. These effects are also noticed in complex hydrides and hydride system [64]. Despite the beneficial effects of milling, there are also some disadvantages. In the case of room temperature hydrides, the effects of milling are not always beneficial. For example, it was also reported that FeTi alloys undergo hydrogen capacity loss after milling process. This is due to the creation of amorphous regions induced by the mechanical deformation and it is not possible to store hydrogen interstitially in the amorphous regions [65]. Furthermore, taking into account that the milling vessel and grinding medium are usually made of stainless steel, Fe contamination is also a concern, particularly at the time to perform the milling process in a high-energy mill device. For instance, as demonstrated by Puszkiel et al., the presence of Fe for the $2LiBH_4 + MgH_2$ hydride system causes detrimental effects in the kinetic behavior since FeB species without any beneficial effects are formed. It was found that an appreciable amount of Fe came mostly from the grinding medium [66]. Despite the described disadvantages, the milling process is quite effective and efficient at the time to prepare and tailor hydride compounds and systems and additionally it is possible to scale-up for practical applications. Reducing the grain and particle sizes, creating more boundary surfaces and defects are the most relevant effects of the milling process. These effects mainly improve the diffusion processes for the hydride formation and decomposition by shortening the diffusion pathways and generating channels for more efficient hydrogen transport.

4.2 Doping with transition metal and transition metal compounds

Since the beginning of the investigations on hydride compounds, it was discovered that the addition of transition metal and metal compounds were able to

improve their kinetic characteristics. The addition of amounts from 1 to 10 wt.% of these transition metals and compounds was performed by milling procedures in most of the cases. Therefore, the “doping strategy” also involves the milling process to reach a high degree of intermixture and microstructural refinement. The doping strategy results in reductions of the hydrogenation and/or dehydrogenation activation energies, changes in the reaction paths and consequently different rate-limiting steps. **Figure 10** shows the concept of doping *via* mechanical milling. As an example, the activation energy for the dehydrogenation process for a bulk hydride MH_x (M = metal) is reduced after adding a transition metal and transition metal compound by milling process, $Ea_1 > Ea_2$.

In the case of room temperature hydrides, the presence of transition metals like Pd and Ni notably improves their activation behavior and kinetic properties. This fact was attributed to the active sites of these transition metals, located on the metal or alloy surface, which facilitated the hydrogen molecule dissociation and penetration across the oxides generated on the metal or alloy surface [67–69]. These hydrides are commonly prepared by arc melting since, as mentioned in Section 4.2, the milling process can cause hydrogen capacity losses.

In 1997, Bogdanović et al. [70] achieved reversible hydrogen uptake and release from $NaAlH_4$ under mild conditions by doping with Ti-based catalyst ($TiCl_3$). However, the catalytic mechanism of the Ti-based catalyst was not clear at those times. In 2015, Züttel et al. [71] reported a work about the catalytic mechanism of Ti-compound in the hydrogen uptake/release of alkali alanates. In this work, based on an atomistic model, it was proposed that Ti works as a bridge to transfer H^- and M^+ ($M^+ \cdots Ti \cdots H^-$) from MAH_4 ($M = Li, Na, K$), reducing their charge separation and thus lowering the activation energies for hydrogenation and dehydrogenation processes.

Among the most interesting hydrides, MgH_2 is very attractive because of its low cost and high gravimetric hydrogen capacity (7.6 wt.%). However, its high thermodynamic stability (74 kJ/mol H_2) required high operative temperature over $300^\circ C$ [25]. Pure MgH_2 has sluggish kinetic behavior. Upon hydrogenation, the rate-limiting step is three-dimensional diffusion controlled contracting volume. This fact is attributed to the low diffusion coefficient of MgH_2 covering fresh Mg; the diffusion coefficient of MgH_2 was found to be three orders of magnitude lower than the one for Mg). Upon dehydrogenation, the rate-limiting step for pristine

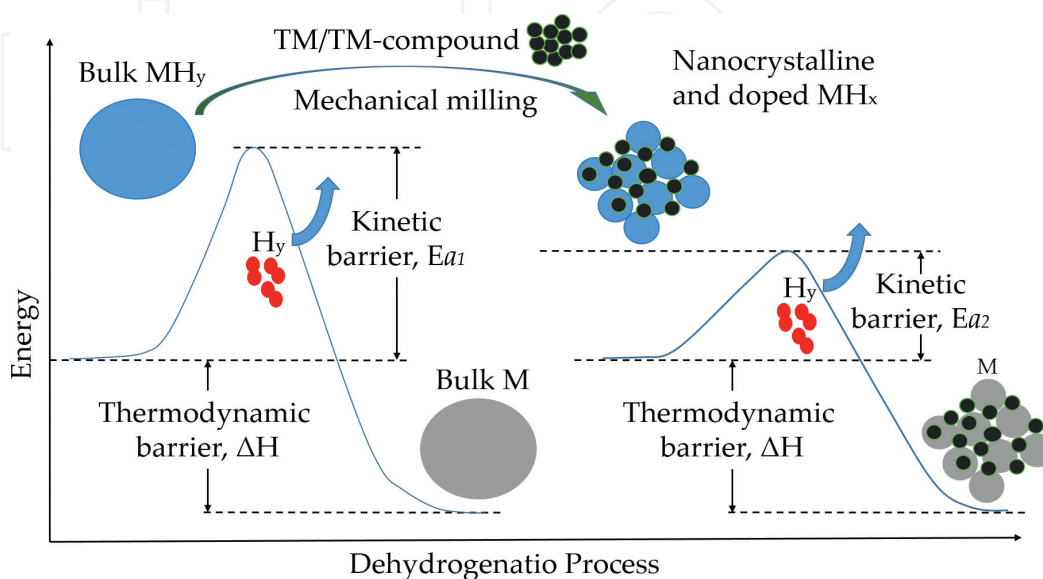


Figure 10.

Concept of doping *via* mechanical milling. TM = transition metal. MH_y = hydride, M = metal, ΔH = enthalpy, Ea = activation energy.

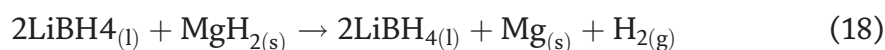
MgH₂ turned to be surface controlled and related to the recombination of the hydrogen molecule [72, 73]. Several transition metals and transition metal compounds exhibited excellent catalytic effect on de-/hydrogenation of MgH₂. The main effect of these additives was related to the dehydrogenation mechanism, since they ease the recombination of the hydrogen molecule [74, 75]. One of the most effective additives was Nb₂O₅, leading to 7 wt.% H₂ capacity in about 60 s and fast dehydrogenation in about 130 s. Moreover, the presence of Nb₂O₅ reduced the dehydrogenation temperature down to 250°C [76]. Nb₂O₅ had a “pathway effect” mainly on the hydrogenation of MgH₂. Upon milling and subsequent hydrogen cycling, the formation of Mg-Nb oxides created diffusion pathways by the formation of metastable niobium hydrides, hence avoiding the large diffusion constraints. The effect and mechanism of Nb₂O₅ on MgH₂ is similar but slower when MgH₂ is physically doped with Nb₂O₅ [77, 78].

LiBH₄ also caught the attention due to the extremely high gravimetric capacity of 18.3 wt.% H₂, though just 13.8 wt.% H₂ is available because LiH and B are formed upon desorption. However, LiBH₄ is quite stable and needs harsh temperature and pressure conditions for de-/re-hydrogenation [79]. Several dopants such as metal oxides and metal halides were tried for improving the kinetic behavior of LiBH₄. However, LiBH₄ reacts with the dopants because this complex hydride is a strong reduction agent. The interactions between LiBH₄ and dopants also lead to gas byproducts such as B₂H₆. In this regard, complex hydrides such as borohydrides and amides are combined with binary hydrides to form “thermodynamically destabilized systems” and then the kinetic behavior of these hydride systems is tailored by doping [30, 31]. In almost all the cases, the added dopants interact with the hydride system itself by forming other species *in situ*, and this strategy will be addressed in the next section.

4.3 *In situ* catalyst formation

This strategy is applied to binary hydrides, to complex hydrides and mainly to destabilized hydride systems. In this section, the *in situ* formation of species with catalytic activity for destabilized hydride system is described. These hydride systems present proper thermodynamic parameters as for example 2LiBH₄ + MgH₂ and Mg(NH₂)₂ + 2LiH, as shown in **Table 2**, because of the exothermic formation of reversible species during the endothermic dehydrogenation. Nonetheless, these hydride systems still present kinetic constraints to reach the operative conditions predicted by the thermodynamic. One of the main strategies to overcome this problem is the addition of dopants. In almost all the cases, these dopants interact with the hydride system by forming *in situ* species with catalytic activity.

One of the most representative examples of this approach is the addition of transition metal compounds to the 2LiBH₄ + MgH₂ hydride system. Under dynamic conditions, this borohydride system uptake hydrogen in one step, but releases hydrogen in two steps as described in reactions (17)–(19), respectively [80].

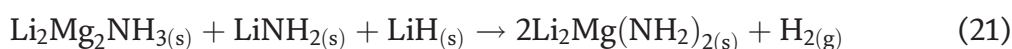


For the hydrogenation process, temperature and pressures of about 350°C and 50 bar are required. These conditions for the formation of LiBH₄ are notably milder than that needed for the re-hydrogenation of LiBH₄ from LiH and B [79]. For the dehydrogenation process, temperatures above 350°C and hydrogen overpressures

higher than 3 bar of hydrogen overpressure are required. These conditions are harsher than those predicted by the thermodynamics (**Table 2**). The hydrogen overpressure upon dehydrogenation assures the reversibility of the hydride system since MgB_2 is only formed under backpressure conditions. As seen in the reactions, LiBH_4 is in liquid state because this complex hydride undergoes from solid to liquid state at about 270°C [81]. Furthermore, mainly upon dehydrogenation the kinetic behavior is sluggish, particularly the second step described by reaction (19), taking more than 10 h for the full hydrogen release. Therefore, one of the most effective strategies was the addition of transition metal compounds [82]. Through this strategy, transition metal halides TiCl_3 , TiF_4 , NbF_5 among others, notably improved the dehydrogenation kinetic behavior of $2\text{LiBH}_4 + \text{MgH}_2$ hydride system. In this case, the transition metal halide additive interacts with LiBH_4 during the preparation stage during milling and subsequent heating to reach the operative temperature for hydrogen interactions. This interaction results in the formation of stable and nanostructure boride species such as TiB_2 and NbB_2 with similar hexagonal crystal structure as MgB_2 . The *in situ* formed nanostructured transition metal boride species act as centers for the nucleation and growth of MgB_2 , hence, accelerating the second step of the dehydrogenation, reaction (19).

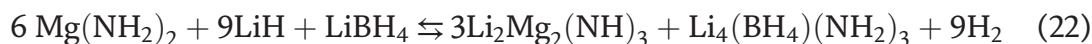
Other example with the same $2\text{LiBH}_4 + \text{MgH}_2$ hydride system is the addition of TiO_2 , leading to the *in situ* formation of core-shell Li_xTiO_2 nanoparticles. The mechanism of these core-shell nanoparticles is different from the one described for transition metal boride species. The core and shell of the nanoparticles are composed of $\text{Li}_{0.59}\text{TiO}_2$ and $\text{Li}_{0.59}\text{TiO}_2$, respectively. Upon hydrogenation and dehydrogenation, the *in situ* formed core-shell nanoparticles works as reversible Li^+ pumps, promoting the early decomposition of LiBH_4 and providing Li^+ for its rehydrogenation. Furthermore, the core-shell Li_xTiO_2 also improve the dehydrogenation of MgH_2 , reaction (18). The addition of 1 wt.% of TiO_2 to $2\text{LiBH}_4 + \text{MgH}_2$ hydride system leads to hydrogen capacities of about 10 wt.% H_2 , markedly shorter uptake (25 min) and release hydrogen times (50 min) and reduced activations energies at 400°C . The rate-limiting step for the hydrogenation process of the $2\text{LiBH}_4 + \text{MgH}_2$ doped with TiO_2 was one-dimensional interface-controlled mechanism (JMA, $n = 1$), while for the pristine material it was generally a diffusion controlled process [82]. As a novel approach, Puszkiel et al. interpreted the two steps dehydrogenation process by the combination of the JMA model with $n = 1$ for the fast MgH_2 decomposing, reaction (18), and the modified autocatalytic Prout-Tompkins model for the decomposition of LiBH_4 /formation of MgB_2 . Therefore, this autocatalytic process accelerated with the further formation of MgB_2 . The nanostructured core-shell Li_xTiO_2 particles prompt the fast formation of MgB_2 seeds by acting as Li^+ sink/source for the early decomposition of LiBH_4 and the subsequent formation of LiH , respectively.

$\text{Mg}(\text{NH}_2)_2 + 2\text{LiH}$ was also investigated as a potential hydrogen storage material due to its hydrogen capacity of about 5 wt.% and operative temperature roughly 220°C [83]. This hydride system uptake/release hydrogen in two steps according to reactions (20) and (21):



Several additives such as halides and hydrides were used to try to improve the kinetic behavior of this system [84–89]. However, it was found that the addition of just 0.1 mol of LiBH_4 improves not only the kinetic behavior, but also reduces the reaction enthalpy from 38.9 to 36.5 kJ/mol H_2 [31, 90]. Moreover, the 6 $\text{Mg}(\text{NH}_2)_2 + 9\text{LiH} + \text{LiBH}_4$ molar composition is the optimum one for the kinetic-

destabilization effect. *In situ* formed complex amide-borohydrides like $\text{Li}_4(\text{BH}_4)(\text{NH}_2)_3$ and $\text{Li}_2(\text{BH}_4)(\text{NH}_2)$ are responsible for improving the kinetic behavior of the hydride system, according to reaction (22) [91]:



Further improvement for the $6 \text{Mg}(\text{NH}_2)_2 + 9\text{LiH} + \text{LiBH}_4$ was achieved by co-adding YCl_3 and Li_3N . The *in situ* formation of nanostructured YH_3 and YB_x upon milling and hydrogen interaction leads to faster kinetic behavior with reduced activation energy and capacities of about 4 wt.% at 90°C . On one hand, *in situ* formed $\text{Li}_4(\text{NH}_2)_3(\text{BH}_4)$ enhances the Li^+ transport, providing a source for the fast formation of the reacting species. On the other hand, nanostructured YB_x species contribute to the dissociation of H_2 [92].

Figure 11 depicts the concepts of the *in situ* catalyst formation applied to “destabilized hydride system.” The complex hydride ABH_y ($A = \text{metal}$, $B = \text{non-metal}$) or metal can react with a binary hydride, MH_x ($M = \text{metal}$; different from A) to lower the thermodynamic stability by the exothermal formation of MB , thus $\Delta H_1 > \Delta H_2$. The *in situ* formation of catalytic species lowers the activation energy, i.e., $Ea_1 > Ea_2$, but does not alter the thermodynamic stability of the system.

4.4 Nanoconfinement

This strategy consists in confining the dimensions of hydride particles to sizes lower than 25 nm by introducing them into a nanoporous matrix. For a simple hydride formation/decomposition reaction (23), the contribution of the excess surface area given by the nanosize of the metal ($M_{(s)}$) and metal hydride ($\text{MH}_{2(s)}$) must be taken into account as part of the reaction enthalpy as described in reaction (24), where V_m is the molar volume, r particle radius and $E(\gamma, r, E_{\text{ads}})$ is the surface energy term which depends on the surface free energies (γ) of the metal hydride and the metal particle, on the molar volumes of the two solid reaction partners, and on an additional energy term E_{ads} , which takes into account that binding of H_2 at the surface of both the metal and the hydride reduce the respective surface energy by minimizing the excess of surface energy (γ) arising from not bound surface atoms. Therefore, the classical van't Hoff equation (Section 2.2, Eq. (4)) is corrected by the effects of nanoconfinement by replacing ΔH for $\Delta H'$, which takes into account the surface effects owing to the nanometric condition of the particles as shown in Eq. (25) [93].

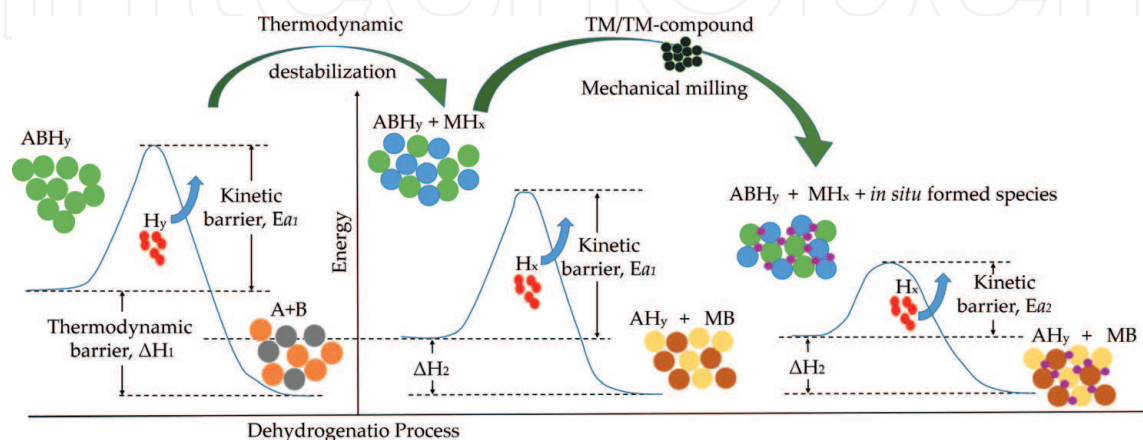


Figure 11. Concept of *in situ* catalyst formation applied to destabilized hydride system. Complex hydride = ABH_y ($A = \text{metal}$, $B = \text{non-metal or metal}$); binary hydride, MH_x ($M = \text{metal}$; different from A ; $\text{TM} = \text{transition metal}$). ΔH = enthalpy, Ea = activation energy.



$$\Delta H' = \Delta H + [(3Vm E(\gamma, r, Eads))/r] \quad (24)$$

$$\ln P_{eq} = \left[\frac{\Delta H'}{RT} \right] - \left[\frac{\Delta S}{R} \right], \quad (25)$$

Nanoconfinement was basically proposed as a promising strategy to make hydride compounds reversible under mild conditions, as for example $LiBH_4$, $NaAlH_4$, and MgH_2 , and to further destabilized hydrogen systems such as $2LiBH_4 + MgH_2$. However, in most of the cases, the main effect was observed on the kinetic behavior of the hydride compounds and systems. The nanometric range of the particles provide extremely large grain boundaries and notable shorter diffusion paths as well as optimized contacting for the materials, hence these properties account for improvements in terms of kinetic behavior and cycling stability. Carbon frames such as scaffolds, nanotubes, and aerogels are used for confining hydrides due to its light weight and inter condition. Despite the fact that this strategy usually leads to improved kinetic behavior without actually changing the thermodynamics of the hydride compound and system, the main constraint lay on the reduced capacity because of the introduction of the hydride into the nanoporous frame. Furthermore, it is hard to figure out in a possible scale-up for practical application [94–96].

5. Conclusions

Hydrogen can be considered as future energy carrier because of its large gravimetric energy density, abundance as combined with oxygen in water and its environmentally friendly condition at the time to release its energy. However, its low volumetric energy density owing to its gas conditions demands an efficient and a safe method to store hydrogen. One of the most attractive methods consists in storing hydrogen in solid state by forming a hydride compound. Much effort has been put in designing hydride forming materials and hydrogen storage systems based on hydride forming materials. One of the main constraints for the design of commercial solid-state hydrogen storage systems is the lack of a hydride forming material able to have proper thermodynamic stability as well as kinetic behavior. There are already materials with suitable experimental thermodynamic properties which would allow to reversibly uptake and release hydrogen at low temperature of about $90^\circ C$ and under low pressures. Nonetheless, these conditions predicted by the thermodynamics of the system cannot be reached because of kinetic constraints. Therefore, strategies to tailor the kinetic behavior of hydride compounds and system of technical interest have been intensively developed. In this chapter, all the basics concepts about the chemical reaction, thermodynamics and kinetics for the right understanding of the solid-state hydrogen storage as hydride compounds or systems were explained. Then, the main strategies to tune the kinetic behavior of hydride compounds or systems were described. Among the most interesting strategies, milling process, transition metal, and transition metal compound doping, *in situ* catalyst formation and nanoconfinement were developed. Despite the fact that several hydrogen storage materials were notably improves by applying the exposed strategies, none of the materials nowadays fulfills the requirements for an efficient, a safe, and a cost effective practical application; hence, there is the need for further research in this field by applying the traditional design strategies and/or by developing new ones.

Acknowledgements

The author acknowledges CONICET (Consejo Nacional de Investigaciones Científicas y Técnicas) and Alexander von Humboldt Foundation (Fellowship Number: ARG-1187279-GF-P).

Conflict of interest


There is no conflict of interest.

Author details

Julián Atilio Puszkiel
National Council of Scientific and Technological Research (CONICET),
San Carlos de Bariloche, Río Negro, Argentina

*Address all correspondence to: julianpuszkiel1979@gmail.com

IntechOpen

© 2018 The Author(s). Licensee IntechOpen. This chapter is distributed under the terms of the Creative Commons Attribution License (<http://creativecommons.org/licenses/by/3.0>), which permits unrestricted use, distribution, and reproduction in any medium, provided the original work is properly cited. 

References

- [1] International Energy Agency. Oil Market Reports <https://www.iea.org/media/omrreports/tables/2013-12-11.pdf>, <https://www.iea.org/media/omrreports/tables/2018-08-10.pdf>
- [2] www.worldenergy.org, https://www.worldenergy.org/wp-content/uploads/2016/10/World-Energy-Resources_FullReport_2016.pdf
- [3] Schlapbach L, Züttel A. Hydrogen-storage materials for mobile applications. *Nature*. 2001;**414**:353-358. DOI: 10.1038/35104634
- [4] Züttel A, Borgschule A, Schlapbach L. Hydrogen as a Future Energy Carrier. 1st ed. WILEY-VCH: Weinheim; 2008. 441 p. DOI: 10.1098/rsta.2010.0113
- [5] Rand DAJ, Dell RM. Hydrogen Energy – Challenges and Prospects. 1st ed. Cambridge: The Royal Society of Chemistry; 2008. 296 p
- [6] Schlapbach L, Züttel A. Hydrogen-storage materials for mobile applications. *Nature*. 2001;**414**:353-358. DOI: 10.1038/35104634
- [7] Turner JA. Sustainable hydrogen production. *Science*. 2004;**305**:972-974. DOI: 10.1126/science.1103197
- [8] Léon A. Hydrogen Technology: Mobile and Portable Applications (Green Energy and Technology). 1st ed. Berlin: Springer; 2008. 184 P. DOI: 10.1007/978-3-540-69925-5
- [9] Graves C, Ebbesen SD, Mogensen M, Lackner KS. Sustainable hydrocarbon fuels by recycling CO₂ and H₂O with renewable or nuclear energy. *Renewable and Sustainable Energy Reviews*. 2011;**15**:1-23. DOI: 10.1016/j.rser.2010.07.014
- [10] Becker WL, Braun RJ, Penev M, Melaina M. Production of Fischer-Tropsch liquid fuels from high temperature solid oxide co-electrolysis units. *Energy*. 2002;**47**:99-115. DOI: 10.1016/j.energy.2012.08.047
- [11] Ebbesen SD, Jensen SH, Hauch A, Mogensen MB. High temperature electrolysis in alkaline cells, solid proton conducting cells, and solid oxide cells. *Chemical Reviews*. 2014;**114**:10697-10734. DOI: 10.1021/cr5000865
- [12] Moller KT, Jensen TR, Akiba E, Li H-w. Hydrogen - A sustainable energy carrier. *Progress in Natural Science*. 2017;**27**(1):34-40. DOI: 10.1016/j.pnsc.2016.12.014
- [13] Barthelemy H, Weber M, Barbier F. Hydrogen storage: Recent improvements and industrial perspectives. *International Journal of Hydrogen Energy*. 2017;**42**(11):7254-7262. DOI: 10.1016/j.ijhydene.2016.03.178
- [14] EU FP6 Integrated Project STORHY. <http://www.storhy.net>
- [15] Sandrock G. A panoramic overview of hydrogen storage alloys from a gas reaction point of view. *Journal of Alloys and Compounds*. 1999;**293-295**:877-888. DOI: 10.1016/S0925-8388(99)00384-9
- [16] S-i O, Nakamori Y, Eliseo JR, Züttel A, Jensen CM. Complex hydrides for hydrogen storage. *Chemical Reviews*. 2007;**107**:4111-4132. DOI: 10.1021/cr0501846
- [17] Puszkiel J, Garroni S, Milanese C, Gennari F, Klassen T, Dornheim M, et al. Tetrahydroborates: Development and potential as hydrogen storage medium. *Inorganics*. 2017;**5**(4):74-97. DOI: 10.3390/inorganics5040074
- [18] Puszkiel J, Andrade-Gamboa J, Gennari FC. Recent progress in Mg-Co-H and Mg-Fe-H systems for hydrogen energy storage applications.

- In: Cheong KY, Impellizzeri G, Fraga M, editors. *Emerging Materials for Energy Conversion and Storage*. 1st ed. Cambridge: Elsevier; 2018. pp. 393-428. DOI: 10.1016/C2017-0-00444-5
- [19] Garroni S, Santoru A, Cao H, Dornheim M, Klassen T, Milanese C, et al. Recent progress and new perspectives on metal amide and imide systems for solid-state hydrogen storage. *Energies*. 2018;**11**:1027-1055. DOI: 10.3390/en11051027
- [20] Milanese C, Garroni S, Gennari F, Marini A, Klassen T, Dornheim M, et al. Solid state hydrogen storage in alanates and alanate-based compounds: A review. *Metals*. 2018;**8**:567-582. DOI: 10.3390/met8080567
- [21] Walker G. Multicomponent hydrogen storage systems. In: Walker G, editor. *Solid –State Hydrogen Storage – Materials and Chemistry*. 1st ed. England: Woodhead Publishing Limited; 2008. pp. 480-482. DOI: 10.1533/9781845694944.4.478
- [22] Rudman PS, Sandrock GD. Metallurgy of rechargeable hydrides. *Annual Review of Materials Science*. 1982;**12**:271-294. DOI: 10.1146/annurev.ms.12.080182.001415
- [23] Schwarz RB, Khachaturyan AG. Thermodynamics of open two-phase systems with coherent interfaces. *Physical Review Letters*. 1995;**74**(13): 2523-2526. DOI: 10.1103/PhysRevLett.74.2523
- [24] Dantzer P, Meuner F. What materials to use in hydride chemical heat pumps? *Materials Science Forum*. 1988;**31**:1-18. DOI: 10.4028/www.scientific.net/MSF.31.1
- [25] Stampfer JF, Holley CE, Suttle JF. The magnesium-hydrogen system. *Journal of the American Chemical Society*. 1960;**82**:7:3504-3508. DOI: 10.1021/ja01499a006
- [26] Puszkiel J, Arneodo Larochette P, Gennari FC. Thermodynamic and kinetic studies of Mg-Fe-H after mechanical milling followed by sintering. *Journal of Alloys and Compounds*. 2008;**463**:134-142. DOI: 10.1016/j.jallcom.2007.08.085
- [27] Maunon P, Buchter F, Friedrichs O, Remhof A, Biemann M, Zwicky CN, et al. Stability and reversibility of LiBH₄. *The Journal of Physical Chemistry. B*. 2008; **112**:906-910. DOI: 10.1021/jp077572r
- [28] Bogdanović B, Brand RA, Marjanović A, Schwickardi M, Tölle J. Metal-doped sodium aluminium hydrides as potential new hydrogen storage materials. *Journal of Alloys and Compounds*. 2000;**302**:36-58. DOI: 10.1016/S0925-8388(99)00663-5
- [29] Chen P, Xiong Z, Luo J, Lin J, Tan KL. Interaction of hydrogen with metal nitrides and imides. *Nature*. 2002;**420**: 302-304. DOI: 10.1038/nature01210
- [30] Vajo JJ, Skeith SK. Reversible storage of hydrogen in destabilized LiBH₄. *The Journal of Physical Chemistry. B*. 2005;**109**:3719-3722. DOI: 10.1021/jp040769o
- [31] Xiong Z, Hu J, Wu G, Chen P, Luo W, Gross K, et al. Thermodynamic and kinetic investigations of the hydrogen storage in the Li-Mg-N-H system. *Journal of Alloys and Compounds*. 2005; **398**:235-239. DOI: 10.1016/j.jallcom.2005.02.010
- [32] Christian JW. *The Theory of Transformations in Metals and Alloys*. 3rd ed. Amsterdam: Pergamon; 2002. 1170 p. In Press
- [33] Khawam A, Flanagan DR. Solid-state kinetic models: Basics and mathematical fundamentals. *The Journal of Physical Chemistry. B*. 2006;**110**:17315-17328. DOI: 10.1021/jp062746a
- [34] Stoch LS. Structural thermochemistry of solids. *Themochim.*

- Acta. 1989;**148**:149-164. DOI: 10.1016/0040-6031(89)85211-6
- [35] Gommel MM, Borkhart C, Fromm E. Absorption and desorption kinetics of hydrogen storage alloys. *Journal of Alloys and Compounds*. 1996;**238**:193-201. DOI: 10.1016/0925-8388(96)02217-7
- [36] Brown ME. The Prout-Tompkins rate equation in solid-state kinetics. *Thermochimica Acta*. 1997;**300**:93-106. DOI: 10.1016/S0040-6031(96)03119-X
- [37] Sharp JH, Brindley GW, Achar BN. Numerical data for some commonly used solid state reaction equations. *Journal of the American Ceramic Society*. 1966;**49**:379-382. DOI: 10.1111/j.1151-2916.1966.tb13289.x
- [38] Jones LF, Dollimore D, Nicklim T. Comparison of experimental kinetic decomposition data with master data using a linear plot method. *Thermochimica Acta*. 1975;**13**:240-245. DOI: 10.1016/0040-6031(75)80085-2
- [39] Höne G, Hemminger W, Flammersheim HJ. *Differential Scanning Calorimetry*. 1st ed. Berlin: Springer; 1996. 188 p. DOI: 10.1007/978-3-662-03302-9_3
- [40] Kissinger HE. Reaction kinetics in differential thermal analysis. *Analytical Chemistry*. 1957;**29**:1702-1706. DOI: 10.1021/ac60131a045
- [41] Wang XL, Suda S. A dehydriding kinetic study of $\text{LaNi}_{4.7}\text{Al}_{0.3}$ hydride by a step-wise method. *Journal of the Less Common Metals*. 1990;**159**:83-90. DOI: 10.1016/0022-5088(90)90135-7
- [42] Yosephy Y, Ron M. Kinetic measurements of LaNi_5H_x and $\text{MnNi}_{4.15}\text{Fe}_{0.85}\text{H}_x$ with constant pressure differential. *Journal of the Less Common Metals*. 1988;**147**:227-238. DOI: 10.1016/0022-5088(89)90196-3
- [43] Reilly JJ, Yosephy Y, Johnson JR. Kinetics of the isothermal decomposition of lanthanum nickel hydride. *Zeitschrift für Physikalische Chemie N.F.* 1989;**164**:1241-1247. DOI: 10.1524/zpch.1989.164.Part_2.1241
- [44] Goodell PD, Rudman PS. Hydriding and dehydriding rates of the $\text{LaNi}_5\text{-H}$ system. *Journal of the Less Common Metals*. 1983;**89**:117-125. DOI: 10.1016/0022-5088(83)90255-2
- [45] Bernauer O, Töpler J, Noreus D, Hempelman R, Richter D. Fundamentals and properties of some Ti/Mn based laves phase hydrides. *International Journal of Hydrogen Energy*. 1989;**14**:187-200. DOI: 10.1016/0360-3199(89)90053-0
- [46] Han JS, Lee J-Y. A study on the dehydriding kinetics of Mg_2Ni intermetallic compound. *Journal of the Less Common Metals*. 1987;**128**:155-165. DOI: 10.1016/0022-5088(87)90201-3
- [47] Kim SR, Lee JY. The effect of thermal cycling on the hydriding rate of $\text{MmNi}_{4.5}\text{Al}_{0.5}$. *Journal of the Less Common Metals*. 1990;**161**:37-47. DOI: 10.1016/0022-5088(90)90312-8
- [48] Karlicek LF, Lowe IJ. Hydrogen diffusion in $\beta\text{-LaNi}_5$ hydride. *Solid State Communications*. 1979;**31**:163-165. DOI: 10.1016/0038-1098(79)90426-5
- [49] Miyamoto M, Yamaji K, Nakata Y. Reaction kinetics of LaNi_5 . *Journal of the Less Common Metals*. 1983;**89**:111-116. DOI: 10.1016/0022-5088(83)90254-0
- [50] Song MY, Pezat M, Darret B. A kinetics study of the $\text{H-(Mg}_2\text{Ni-2.7wt.\% Ni)}$ system. *Journal of the Less Common Metals*. 1984;**103**:145-152. DOI: 10.1016/0022-5088(84)90373-4
- [51] Fernández JF, Sánchez CR. Rate limiting step in the absorption and desorption of hydrogen by magnesium. *Journal of Alloys and Compounds*. 2002;**340**:189-198. DOI: 10.1016/S0925-8388(02)00120-2

- [52] Jepsen J, Milanese C, Puszkiel J, Girella A, Schiavo B, Lozano GA, et al. Fundamental material properties of the $2\text{LiBH}_4\text{-MgH}_2$ reactive hydride composite for hydrogen storage: (II) Kinetic properties. *Energies*. 2018;**11**: 1170(15). DOI: 10.3390/en11051081
- [53] Ushida HH, Fromm E: H_2 absorption rate of titanium films contaminated with increasing amounts of N_2 , H_2O , CO , CO_2 , CH_2 and SO_2 . *Zeitschrift für Physikalische Chemie N.F.* 1989;**164**:1123–1128. DOI: 10.1524/zpch.1989.164.Part_2.1123
- [54] Bershadsky E. Investigation of kinetics and structural changes in $\text{TiFe}_{0.8}\text{Ni}_{0.2}$ after prolonged cycling. *Journal of the Less Common Metals*. 1991;**172-174**:1036-1043. DOI: 10.1016/S0022-5088(06)80009-3
- [55] Rudman PS. Hydrogen-diffusion-rate-limited hydriding and dehydriding kinetics. *Journal of Applied Physics*. 1979;**50**(11):7195-7199. DOI: 10.1063/1.325831
- [56] Lozano GA, Ranong CN, Bellosta von Colbe JM, Bormann R, Fieg G, Hapke J, et al. Empirical kinetic model of sodium alanate reacting system (I). hydrogen absorption. *International Journal of Hydrogen Energy*. 2010;**35**: 6763-6772. DOI: 10.1016/j.ijhydene.2010.04.080
- [57] Ley MB, Meggouh M, Moury R, Peinecke K, Felderhoff M. Development of hydrogen storage tank systems based on complex metal hydrides. *Materials*. 2015;**8**:5891-5921. DOI: 10.3390/ma8095280
- [58] Suryanarayana C. Mechanical alloying and milling. *Progress in Materials Science*. 2001;**46**:1-184. DOI: 10.1016/S0079-6425(99)00010-9
- [59] Huot J, Ravnsbæk DB, Zhang J, Cuevas F, Latroche M, Jensen TR. Mechanochemical synthesis of hydrogen storage materials. *Progress in Materials Science*. 2013;**58**:30-75. DOI: 10.1016/j.pmatsci.2012.07.001
- [60] Abdellaoui M, Gaffet E. The physics of mechanical alloying in a planetary ball mill: Mathematical treatment. *Acta Metallurgica et Materialia*. 1995;**43**: 1087-1098. DOI: 10.1016/0956-7151(95)92625-7
- [61] Puszkiel JA, Gennari FC, Arneodo Larochette P. Synthesis of Mg_{15}Fe materials for hydrogen storage applying ball milling procedures. *Journal of Alloys and Compounds*. 2010;**495**: 655-658. DOI: 10.1016/j.jallcom.2009.10.011
- [62] Puszkiel JA, Arneodo Larochette P, Gennari FC. Hydrogen storage properties of Mg_xFe (x: 2, 3 and 15) compounds produced by reactive ball milling. *Journal of Power Sources*. 2009;**186**:185-193. DOI: 10.1016/j.jpowsour.2008.09.101
- [63] Zaluski L, Zaluska A, Ström-Olsen JO. Nanocrystalline metal hydrides. *Journal of Alloys and Compounds*. 1997;**253-254**:70-79. DOI: 10.1016/S0925-8388(96)02985-4
- [64] Varin RA, Czujko T, Wronsky ZS. *Nanomaterials for Solid State hydrogen Storage*. 1st ed. New York: Springer; 2009. . 325 p. DOI: 10.1007/978-0-387-77712-2
- [65] Haraki T, Oishi K, Uchida H, Miyamoto Y, Abe M, Kokaji T, et al. Properties of hydrogen absorption by nano-structured FeTi alloys. *International Journal of Materials Research*. 2008;**99**:507-512. DOI: 10.3139/146.101669
- [66] Puszkiel JA, Gennari FC, Arneodo Larochette P, Ramallo-López JM, Vainio U, Karimi F, et al. Effect of Fe additive on the hydrogenation-dehydrogenation properties of $2\text{LiH} + \text{MgB}_2/2\text{LiBH}_4 + \text{MgH}_2$ system. *Journal of Power Sources*.

2015;**284**:606-616. DOI: 10.1016/j.jpowsour.2015.02.153

[67] Bratanich TI, Solonin SM, Skorokhod VV. Mechanical activation of hydrogen sorption with intermetallic compounds LaNi_5 and TiFe in powder systems. *International Journal of Hydrogen Energy*. 1995;**20**(5):353-355. DOI: 10.1016/0360-3199(94)00062-5

[68] Chung HS, Lee JY. Hydriding and dehydriding reaction rate of FeTi intermetallic compound. *International Journal of Hydrogen Energy*. 1985;**10**(7-8):537-542. DOI: 10.1016/0360-3199(85)90084-9

[69] Kulshreshtha SK, Jayakumar OD, Bhatt KB. Hydriding characteristics of palladium and platinum alloyed FeTi . *Journal of Materials Science*. 1993; **28**(15):4229-4233. DOI: 10.1007/BF00351259

[70] Bogdanović B, Schwickardi M. Ti-doped alkali metal aluminum hydrides as potential novel reversible hydrogen storage materials. *Journal of Alloys and Compounds*. 1997;**253**:1-9. DOI: 10.1016/S0925-8388(96)03049-6

[71] Atakli ZÖK, Callini E, Kato S, Mauron P, Orimo S-I, Züttel A. The catalyzed hydrogen sorption mechanism in alkali alanates. *Physical Chemistry Chemical Physics*. 2015;**17**:20932-20940. DOI: 10.1039/c5cp01684c

[72] Barkhordarian G, Klassen T, Bormann R. Kinetic investigation of the effect of milling time on the hydrogen sorption reaction of magnesium catalyzed with different Nb_2O_5 contents. *Journal of Alloys and Compounds*. 2006;**407**:249-255. DOI: 10.1016/j.jallcom.2005.05.037

[73] Evard E, Gabis I, Yartys VA. Kinetics of hydrogen evolution from MgH_2 : Experimental studies, mechanism and modelling. *International Journal of Hydrogen Energy*. 2010;**35**(17):9060-9069. DOI: 10.1016/j.ijhydene.2010.05.092

[74] Liang G, Huot J, Boily S, Van Neste A, Schulz R. Catalytic effect of transition metals on hydrogen sorption in nanocrystalline ball milled MgH_2 -Tm (Tm=Ti, V, Mn, Fe and Ni) systems. *Journal of Alloys and Compounds*. 1999; **292**:247-252

[75] Barkhordarian G, Klassen T, Bormann R. Catalytic mechanism of transition-metal compounds on Mg hydrogen sorption reaction. *The Journal of Physical Chemistry. B*. 2006;**110**(22): 11020-11024. DOI: 10.1021/jp0541563

[76] Barkhordarian G, Klassen T, Bormann R. Fast hydrogen sorption kinetics of nanocrystalline Mg using Nb_2O_5 as catalyst. *Scripta Materialia*. 2003;**49**:213-217. DOI: 10.1016/S1359-6462(03)00259-8

[77] Friedrichs O, Aguey-Zinsou F, Ares Fernandez JR, Sanchez-Lopez JC, Justo A, Klassen T, et al. MgH_2 with Nb_2O_5 as additive for hydrogen storage: Chemical, structural and kinetic behaviour with heating. *Acta Materialia*. 2006;**54**:105-110. DOI: 10.1016/j.actamat.2005.08.024

[78] Friedrichs O, Martinez-Martinez D, Guilera G, Sanchez-Lopez JC, Fernandez A. In situ energy-dispersive XAS and XRD study of the superior hydrogen storage system $\text{MgH}_2/\text{Nb}_2\text{O}_5$. *Journal of Physical Chemistry C*. 2007;**111**(28): 10700-10706. DOI: 10.1021/jp0675835

[79] Züttel A, Wenger P, Rentsch S, Sudan P, Mauron P, Emmenegger C. LiBH_4 a new hydrogen storage material. *Journal of Power Sources*. 2003;**118**:1-7. DOI: 10.1016/S0378-7753(03)00054-5

[80] Bösenberg U, Doppiu S, Mosegaard L, Barkhordarian G, Eigen N, Borgschulte A, et al. Hydrogen sorption properties of MgH_2 - LiBH_4 composites. *Acta Materialia*. 2007;**55**:3951-3958. DOI: 10.1016/j.actamat.2007.03.010

[81] Nakagawa T, Ichikawa T, Hanada N, Kojima Y, Fujii H. Thermal analysis

- on the Li-Mg-B-H systems. *Journal of Alloys and Compounds*. 2007;**446**: 306-309. DOI: 10.1016/j.jallcom.2007.02.097
- [82] Bösenberg U, Kim JW, Gosslar D, Eigen N, Jensen TR, Bellosta von Colbe JM, et al. Role of additives in LiBH_4 - MgH_2 reactive hydride composites for sorption kinetics. *Acta Materialia*. 2010; **58**:3381-3389. DOI: 10.1016/j.actamat.2010.02.012
- [83] Leng HY, Ichikawa T, Hino S, Hanada N, Isobe S. New metal-N-H system composed of $\text{Mg}(\text{NH}_2)_2$ and LiH for hydrogen storage. *The Journal of Physical Chemistry. B*. 2004;**108**: 8763-8765. DOI: 10.1021/jp048002j
- [84] Torre F, Valentoni A, Milanese C, Pistidda C, Marini A. Kinetic improvement on the CaH_2 -catalyzed $\text{Mg}(\text{NH}_2)_2 + 2\text{LiH}$ system. 2014;**645**:S284-S287. DOI: 10.1016/j.jallcom.2014.12.228
- [85] Amica G, Enzo S, Larochette PA, Gennari FC. Improvements in the hydrogen storage properties of the $\text{Mg}(\text{NH}_2)_2$ -LiH composite by KOH addition. *Physical Chemistry Chemical Physics*. 2018;**20**:15358-15367. DOI: 10.1039/c8cp02347f
- [86] Liang C, Liu Y, Wei Z, Jiang Y, Gao M. Enhanced dehydrogenation/hydrogenation kinetics of the $\text{Mg}(\text{NH}_2)_2$ -2LiH system with NaOH additive. *International Journal of Hydrogen Energy*. 2011;**36**:2137-2144. DOI: 10.1016/j.ijhydene.2010.11.068
- [87] Li C, Liu Y, Gu Y, Gao M, Pan H. Improved hydrogen-storage thermodynamics and kinetics for an RbF-doped $\text{Mg}(\text{NH}_2)_2$ -2 LiH system. *Chemistry – An Asian Journal*. 2013;**8**: 2136-2143. DOI: 10.1002/asia.201300323
- [88] Li C, Liu Y, Ma R, Zhang X, Li Y. Superior dehydrogenation/hydrogenation kinetics and long-term cycling performance of K and Rb Cocatalyzed $\text{Mg}(\text{NH}_2)_2$ -2LiH system. *ACS Applied Materials & Interfaces*. 2014;**6**: 17024-17033. DOI: 10.1021/am504592x
- [89] Cao H, Wang H, He T, Wu G, Xiong Z, Qiu J, et al. Improved kinetics of the $\text{Mg}(\text{NH}_2)_2$ -2LiH system by addition of lithium halides. *RSC Advances*. 2014;**4**: 32555-32561. DOI: 10.1039/C4RA02864C
- [90] Hu J, Liu Y, Wu G, Xiong Z, Chua YS. Improvement of hydrogen storage properties of the Li-Mg-N-H system by addition of LiBH_4 . *Chemistry of Materials*. 2008;**20**:4398-4402. DOI: 10.1021/cm800584x
- [91] Wang H, Cao H, Wu G, He T, Chen P. The improved hydrogen storage performances of the multi-component composite: $2\text{Mg}(\text{NH}_2)_2$ -3LiH- LiBH_4 . *Energies*. 2015;**8**:6898-6909. DOI: 10.3390/en8076898
- [92] Cao H, Zhang W, Pistidda C, Puzskiel J, Milanese C, Santoru A, et al. Kinetic alteration of the $6\text{Mg}(\text{NH}_2)_2$ -9LiH- LiBH_4 system by co-adding YCl_3 and Li_3N . *Physical Chemistry Chemical Physics*. 2017;**19**:32105-32115. DOI: 10.1039/C7CP06826C
- [93] Fichtner M. Properties of nanoscale metal hydrides. *Nanotechnology*. 2009; **20**:204009-204013. DOI: 10.1088/0957-4484/20/20/204009
- [94] Vajo JJ. Influence of nano-confinement on the thermodynamics and dehydrogenation kinetics of metal hydrides. *Current Opinion in Solid State & Materials Science*. 2011;**15**:52-61. DOI: 10.1016/j.cossms.2010.11.001
- [95] Nielsen KN, Besenbacher F, Jensen TR. Nanoconfined hydrides for energy storage. *Nanoscale*. 2011;**3**:2086-2098. DOI: 10.1039/C0NR00725K
- [96] Yu X, Tang Z, Suna D, Ouyang L, Zhu M. Recent advances and remaining challenges of nanostructured materials for hydrogen storage applications. *Progress in Materials Science*. 2017;**88**: 1-48. DOI: 10.1016/j.pmatsci.2017.03.001